











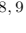
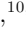








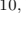




## Single-Star Warm-Jupiter Systems Tend to Be Aligned, Even Around Hot Stellar Hosts: No $T_{\text{eff}}-\lambda$ Dependency\*

XIAN-YU WANG <sup>1</sup>, MALENA RICE <sup>2</sup>, SONGHU WANG <sup>1</sup>, SHUBHAM KANODIA <sup>3</sup>, FEI DAI <sup>4</sup>, SARAH E. LOGSDON <sup>5</sup>,  
HEIDI SCHWEIKER <sup>5</sup>, JOHANNA K. TESKE <sup>3,6</sup>, R. PAUL BUTLER <sup>3</sup>, JEFFREY D. CRANE <sup>6</sup>, STEPHEN SHECTMAN <sup>6</sup>,  
SAMUEL N. QUINN <sup>7</sup>, VESELIN KOSTOV <sup>8,9</sup>, HUGH P. OSBORN <sup>10,11</sup>, ROBERT F. GOEKE <sup>10</sup>, JASON D. EASTMAN <sup>7</sup>,  
AVI SHPORER <sup>10</sup>, DAVID RAPETTI <sup>12,13</sup>, KAREN A. COLLINS <sup>7</sup>, CRISTILYN N. WATKINS <sup>14</sup>, HOWARD M. RELLES <sup>14</sup>,  
GEORGE R. RICKER <sup>10</sup>, SARA SEAGER <sup>10,15,16</sup>, JOSHUA N. WINN <sup>17</sup> AND JON M. JENKINS <sup>12</sup>

<sup>1</sup>Department of Astronomy, Indiana University, 727 East 3rd Street, Bloomington, IN 47405-7105, USA

<sup>2</sup>Department of Astronomy, Yale University, 219 Prospect Street, New Haven, CT 06511, USA

<sup>3</sup>Carnegie Institution for Science, Earth & Planets Laboratory, 5241 Broad Branch Road NW, Washington, DC 20015, USA

<sup>4</sup>Institute for Astronomy, University of Hawai'i, 2680 Woodlawn Drive, Honolulu, Hawaii 96822, USA

<sup>5</sup>NSF's National Optical-Infrared Astronomy Research Laboratory, 950 N. Cherry Ave., Tucson, AZ 85719, USA

<sup>6</sup>The Observatories of the Carnegie Institution for Science, 813 Santa Barbara Street, Pasadena, CA 91101, USA

<sup>7</sup>Center for Astrophysics | Harvard & Smithsonian, 60 Garden Street, Cambridge, MA 02138, USA

<sup>8</sup>NASA Goddard Space Flight Center, 8800 Greenbelt Rd, Greenbelt, MD 20771, USA

<sup>9</sup>SETI Institute, 189 Bernardo Ave, Suite 200, Mountain View, CA 94043, USA

<sup>10</sup>Department of Physics and Kavli Institute for Astrophysics and Space Research, Massachusetts Institute of Technology, Cambridge, MA 02139, USA

<sup>11</sup>Physics Institute, Universität Bern, Gesellschaftsstrasse 6, 3012 Bern, Switzerland

<sup>12</sup>NASA Ames Research Center, Moffett Field, CA 94035, USA

<sup>13</sup>Research Institute for Advanced Computer Science, Universities Space Research Association, Washington, DC 20024, USA

<sup>14</sup>Center for Astrophysics | Harvard & Smithsonian, 60 Garden Street, Cambridge, MA 02138, USA

<sup>15</sup>Department of Earth, Atmospheric and Planetary Sciences, Massachusetts Institute of Technology, Cambridge, MA 02139, USA

<sup>16</sup>Department of Aeronautics and Astronautics, MIT, 77 Massachusetts Avenue, Cambridge, MA 02139, USA

<sup>17</sup>Department of Astrophysical Sciences, Princeton University, 4 Ivy Lane, Princeton, NJ 08544, USA

### ABSTRACT

The stellar obliquity distribution of warm-Jupiter systems is crucial for constraining the dynamical history of Jovian exoplanets, as the warm Jupiters' tidal detachment likely preserves their primordial obliquity. However, the sample size of warm-Jupiter systems with measured stellar obliquities has historically been limited compared to that of hot Jupiters, particularly in hot-star systems. In this work, we present newly obtained sky-projected stellar obliquity measurements for warm-Jupiter systems, TOI-559, TOI-2025, TOI-2031, TOI-2485, TOI-2524, and TOI-3972, derived from the Rossiter–McLaughlin effect, and show that all six systems display alignment with a median measurement uncertainty of  $13^\circ$ . Combining these new measurements with the set of previously reported stellar obliquity measurements, our analysis reveals that single-star warm-Jupiter systems tend to be aligned, even around hot stellar hosts. This alignment exhibits a  $3.4\text{-}\sigma$  deviation from the  $T_{\text{eff}}-\lambda$  dependency observed in hot-Jupiter systems, where planets around cool stars tend to be aligned, while those orbiting hot stars show considerable misalignment. The current distribution of spin-orbit measurements for Jovian exoplanets indicates that misalignments are neither universal nor primordial phenomena affecting all types of planets. The absence of misalignments in single-star warm-Jupiter systems further implies that many hot Jupiters, by contrast, have experienced a dynamically violent history.

Corresponding author: Songhu Wang

sw121@iu.edu

\* This paper includes data gathered with the 6.5 meter Magellan Telescopes located at Las Campanas Observatory, Chile.

*Keywords:* planetary alignment (1243), exoplanet dynamics (490), star-planet interactions (2177), exoplanets (498), planetary theory (1258), exoplanet systems (484)

## 1. INTRODUCTION

The Solar System planets lie on near-coplanar orbits that are close to alignment (within  $\sim 6^\circ$ ) with the Sun’s equator, offering a seemingly coherent framework for planetary formation (Kant 1755; de Laplace 1796). In contrast, the landscape of exoplanetary systems is remarkably varied, showing a puzzling range of spin-orbit orientations for hot Jupiters (see Winn & Fabrycky 2015; Triaud 2018; Albrecht et al. 2022 and references within). The origins of these orbital misalignments have sparked a contentious debate: are misalignments a unique feature of hot-Jupiter systems due to their specific formation processes and dynamical histories, including planet-planet scattering (Rasio & Ford 1996; Beugé & Nesvorný 2012), Kozai-Lidov oscillations (Wu & Murray 2003; Fabrycky & Tremaine 2007; Naoz 2016), and secular interactions (Wu & Lithwick 2011; Petrovich 2015a)? Or, do they instead hint at more ubiquitous processes, such as chaotic accretion (Bate et al. 2010; Thies et al. 2011; Fielding et al. 2015; Bate 2018), magnetic warping (Foucart & Lai 2011; Lai et al. 2011; Romanova et al. 2013, 2021), tilting by a companion star (Borderies et al. 1984; Lubow & Ogilvie 2000; Batygin 2012; Matsakos & Königl 2017), or internal-gravity-wave-induced tumbling (Lai 2012; Lin & Ogilvie 2017; Damiani & Mathis 2018), that may affect a wide array of planetary systems?

The relationship between the spin-orbit orientation of a system and the stellar host’s properties adds another layer to the mystery. Previous studies have demonstrated that hot Jupiters around hot stars, which possess thin convective envelopes and experience rapid rotation, span a wide range of spin-orbit angles, while those around cool stars tend to be aligned (Schlaufman 2010; Winn et al. 2010). Could this trend indicate that tidal interactions have played a significant role in realigning the cool-star systems (Albrecht et al. 2012; Rogers & Lin 2013; Xue et al. 2014; Valsecchi & Rasio 2014; Li & Winn 2016; Anderson et al. 2021; Wang et al. 2021; Rice et al. 2022a; Spalding & Winn 2022; Zanazzi et al. 2024)? Or, could this trend arise due to hot-star systems being dynamically “hotter” – that is, could it be that these systems are more likely to form multi-giant planet systems, subsequently leading to inclination excitation from post-disk dynamical interactions (Wu et al. 2023)?

Warm Jupiters, defined in this work as wide-orbiting ( $11 \leq a/R_* \leq 200$ ) Jovian-mass ( $0.3M_J \leq M_P \leq 13M_J$ ) planets<sup>1</sup>, offer a compelling lens through which to scrutinize these questions. The comparatively wider orbital separations of warm Jupiters make them less prone to tidal realignment than hot Jupiters – which fall within the same mass range, but lie within  $a/R_* < 11$  – such that they do not suffer from the same tidal realignment degeneracy that plagues interpretations of aligned hot Jupiters (Rice et al. 2021). Additionally, warm Jupiters seem less likely to have undergone high-eccentricity migration — a leading theory for hot Jupiter migration (see Dawson & Johnson 2018 and references within) — making them even more valuable for teasing apart the origins and evolution of spin-orbit misalignment.

Historically, the scarcity of spin-orbit measurements for warm Jupiters has stemmed from observational challenges, including the day/night cycle and weather limitations of ground-based transit surveys (e.g., SuperWASP, Pollacco et al. 2006; HATNet, Bakos et al. 2004; HATSouth, Bakos et al. 2013; TrES, Alonso et al. 2004; KELT, Pepper et al. 2007; XO, McCullough et al. 2005 and, CSTAR, Wang et al. 2014) and the *Kepler* mission’s “long stare” observing strategy that identified transiting planets primarily around fainter host stars (Borucki et al. 2010), which are not conducive to precise follow-up studies of wide-orbiting planets with long transits. However, this landscape has been transformed by the advent of the *K2* (Howell et al. 2014) and *TESS* (Ricker et al. 2015) missions, which have successfully identified warm Jupiters around brighter host stars across the sky (e.g., K2-99 b, Smith et al. 2017; K2-114 b and K2-115 b, Shporer et al. 2017; K2-140 b, Giles et al. 2018; K2-232 b, Brahm et al. 2018; TOI-481 b and TOI-892 b, Brahm et al. 2020; TOI-558 b and TOI-559 b, Ikwut-Ukwa et al. 2022, TOI-1478 b,

<sup>1</sup> The  $0.3M_J$  or  $100M_\oplus$  minimum mass limit was adopted following Helled (2023), and is further motivated by the identified transition region around  $95 - 150M_\oplus$  from a series of statistical analyses (e.g., Weiss & Marcy 2014; Hatzes & Rauer 2015; Chen & Kipping 2017; Bashi et al. 2017; Müller et al. 2024). The upper mass limit is set to  $13M_J$ , the minimum mass required for a brown dwarf to ignite deuterium fusion. We use the  $a/R_* = 11$  division between hot and warm Jupiters throughout this work as a cutoff that has been empirically identified, following Rice et al. (2022b), and that concurs with physically motivated limits for efficient tidal realignment (see e.g. Figure 11 of Zanazzi et al. 2024).

Table 1. Log of Observations

Spectroscopy Observations <sup>a</sup>									
Name	Facility/Instrument	Time (UT)	N <sup>b</sup>	Exposure time (s)	Seeing ( $''$ )	Airmass	Moon Phase (%)	Moon Distance ( $^{\circ}$ )	S/N <sup>c</sup>
In-Transit									
TOI-559	Magellan II/PFS	2023-09-26 03:16:41 - 09:10:21	15	1520	1.4-2.0	1.00-1.74	79	76	46
TOI-2025	WIYN/NEID	2023-06-14 04:42:20 - 11:04:24	20	1123	1.2-2.3	1.62-1.75	15	79	20
TOI-2031	WIYN/NEID	2023-10-17 01:46:26 - 07:41:43	16	1290	0.7-1.4	1.54-1.70	3	76	23
TOI-2485	WIYN/NEID	2023-04-06 03:00:02 - 10:50:09	16	1800	0.3-2.0	1.01-2.69	99	31	50
TOI-2524	WIYN/NEID	2024-03-20 02:32:06 - 08:32:32	18	1200	0.8-1.6	1.21-2.24	79	41	11
TOI-3972	WIYN/NEID	2022-12-21 03:15:02 - 08:06:24	18	1000	0.6-1.1	1.16-2.18	13	65	27
TOI-2025	NOT/FIES	2021-08-08 22:06:23 - 03:37:09 <sup>d</sup>	16		Knudstrup et al. (2022)				
Out-of-Transit									
TOI-559	FLWO/TRES	2019-01-28 - 2019-09-12	3		Ikwut-Ukwa et al. (2022)				
TOI-559	CTIO/CHIRON	2019-01-27 - 2019-09-20	22		Ikwut-Ukwa et al. (2022)				
TOI-2025	FLWO/TRES	2020-07-30 - 2021-04-13	16		Rodriguez et al. (2023)				
TOI-2025	NOT/FIES	2020-10-01 - 2022-06-02	39		Knudstrup et al. (2022)				
TOI-2025	WIYN/NEID	2023-04-04 - 2023-04-04	6						
TOI-2524	CTIO/CHIRON	2020-12-26 - 2021-03-09	8		Eberhardt et al. (2023)				
TOI-3972	WIYN/NEID	2023-10-18 - 2024-01-29	13						
TESS Observations									
Name	Sector (source, cadence in seconds)								
TOI-559	04 (TESS-SPOC, 1800); 31 (SPOC, 120)								
TOI-2025	14 (TESS-SPOC, 1800); 18 (TESS-SPOC, 1800); 19 (TESS-SPOC, 1800); 20 (TESS-SPOC, 1800); 24 (TESS-SPOC, 1800);								
TOI-2025	25 (TESS-SPOC, 1800); 26 (TESS-SPOC, 1800); 40 (SPOC, 120); 47 (SPOC, 120); 52 (SPOC, 120); 53 (SPOC, 120);								
TOI-2025	58 (SPOC, 120); 59 (SPOC, 120); 60 (SPOC, 120); 74 (SPOC, 20)								
TOI-2031	18 (TESS-SPOC, 1800); 19 (TESS-SPOC, 1800); 24 (TESS-SPOC, 1800); 25 (TESS-SPOC, 1800); 26 (TESS-SPOC, 1800);								
TOI-2031	52 (SPOC, 120); 53 (SPOC, 120); 58 (SPOC, 120); 59 (SPOC, 120); 60 (SPOC, 120); 73 (SPOC, 120)								
TOI-2485	23 (TESS-SPOC, 1800); 50 (TESS-SPOC, 600)								
TOI-2524	09 (QLP, 1800); 35 (QLP, 600); 45 (SPOC, 120); 46 (SPOC, 120); 62 (SPOC, 120); 72 (SPOC, 120)								
TOI-3972	17 (TESS-SPOC, 1800); 18 (TESS-SPOC, 1800); 24 (TESS-SPOC, 600); 58 (SPOC, 120)								
Ground-Based Photometric Follow-Up Observations									
Name	Facility/Instrument	Aperture (m)	Filter	Date (UT)	Exposure time (s)	Source			
TOI-559	PEST	0.3048	Rc	2019-09-27	60	Ikwut-Ukwa et al. (2022)			
TOI-559	LCOGT SSO	1.0	Sloan z'	2019-10-18	35	Ikwut-Ukwa et al. (2022)			
TOI-559	LCOGT SSO	1.0	Sloan i'	2020-08-20	25	Ikwut-Ukwa et al. (2022)			
TOI-559	LCOGT SSO	1.0	Sloan i'	2020-08-27	25	Ikwut-Ukwa et al. (2022)			
TOI-2025	Kotizarovci	0.3	TESS	2020-06-26	30	Knudstrup et al. (2022); Rodriguez et al. (2023)			
TOI-2025	LCOGT TFN	0.4	g'	2020-06-26	60	Knudstrup et al. (2022); Rodriguez et al. (2023)			
TOI-2025	FLWO/KeplerCam	1.2	B	2021-05-12	20	Knudstrup et al. (2022); Rodriguez et al. (2023)			
TOI-2025	FLWO/KeplerCam	1.2	i'	2021-05-12	7	Knudstrup et al. (2022); Rodriguez et al. (2023)			
TOI-2025	GMU	0.8	R	2021-05-12	50	Knudstrup et al. (2022); Rodriguez et al. (2023)			
TOI-2025	CRCAO	0.61	R	2021-05-12	120	Knudstrup et al. (2022); Rodriguez et al. (2023)			
TOI-2025	CPO	0.61	V	2021-09-18	30	Knudstrup et al. (2022); Rodriguez et al. (2023)			
TOI-2025	LCOGT McD	0.35	zs	2023-06-14	55	This work			
TOI-2524	El Sauce	0.36	R <sub>c</sub>	2021-03-31	180	Eberhardt et al. (2023)			
TOI-2031	LCOGT McD	0.35	ip	2023-07-05	70	This work			

<sup>a</sup> For already-published data, we have added the corresponding reference at the end of each data row.

<sup>b</sup> The number of exposures.

<sup>c</sup> Typical signal-to-noise (S/N) at 5530 Å for NEID and in the iodine region (5010 - 6010 Å) for PFS.

<sup>d</sup> This observation started on UT 2021-08-08 at 22:06:23 and ended on UT 2021-08-09 at 03:37:09.

Rodriguez et al. 2021, and 55 warm Jupiter candidates listed in Dong et al. 2021).

In this context, the Stellar Obliquities in Long-period Exoplanet Systems (SOLES) survey (Rice et al. 2021; Wang et al. 2022; Rice et al. 2022b, 2023a; Hixenbaugh et al. 2023; Dong et al. 2023; Wright et al. 2023; Rice et al. 2023b; Lubin et al. 2023; Hu et al. 2024; Radzom et al. 2024; Ferreira et al. 2024) was initiated to broaden the sample of Rossiter–McLaughlin (RM) measurements, especially for planets with wide orbital separations. This paper represents the most recent contributions from the SOLES survey, adding six new spin-orbit angle measurements for warm Jupiters (TOI-559 b, TOI-2025 b, TOI-2031 b, TOI-2485 b, TOI-2524 b, and TOI-3972 b<sup>2</sup>) that orbit hosts spanning a range of stellar types. Our findings reinforce the recent evidence that warm Jupiters in single-star systems are preferentially aligned relative to hot Jupiters, as first demonstrated by Rice et al. (2022b). We crucially extend this observation to demonstrate the same trend for warm Jupiters around hot stars, showing a 3.4- $\sigma$  confidence difference with the  $T_{\text{eff}}-\lambda$  dependency observed in hot-Jupiter systems.

## 2. OBSERVATIONS

### 2.1. Spectroscopy Observation

#### 2.1.1. PFS observation

The transit spectroscopy sequence across the transit of TOI-559 b was conducted during UT September 26, 2023, using the Carnegie Planet Finder Spectrograph (PFS, Crane et al. 2006; Crane et al. 2008, 2010) on the 6.5 m Magellan Clay telescope at Las Campanas Observatory (LCO), Chile. PFS, which has been on-sky since 2010, covers wavelengths from 391 to 734 nm with a default resolving power of  $\sim 127,000$  ( $1 \times 2$  binning and  $0.3''$  slit). In our case, due to the faint magnitude of the star, we used  $3 \times 3$  binning, resulting in a resolving power of  $\sim 110,000$ . Our observing sequence provided a total of 15 RVs each with an exposure time of 1520 seconds, obtained with a moon phase of 79% and a  $76^\circ$  separation between the moon and TOI-559. Seeing ranged from  $1.4 - 2''$ . We also obtained an iodine-free template observation with PFS, which consisted of three 1000-second exposures during UT November 11, 2023 with seeing  $0.55''$ .

<sup>2</sup> The Jovian natures of TOI-2031 b, TOI-2485 b, and TOI-3972 b have been confirmed in Yee et al. (2024, in prep), Carleo et al. (2024), and Schulte et al. (2024, in prep), respectively.

The spectral data reduction and radial velocity (RV) extraction for PFS spectra were performed using a customized pipeline described in Butler et al. (1996).

#### 2.1.2. NEID observation

The transit spectroscopy observations of TOI-2025 b, TOI-2031 b, TOI-2485 b, TOI-2524 b and TOI-3972 b were conducted using the High-Resolution mode ( $R \sim 110,000$ ) of the NEID spectrograph (Schwab et al. 2016; Halverson et al. 2016) on the WIYN 3.5m telescope at Kitt Peak National Observatory in Arizona, USA. The fiber-fed (Kanodia et al. 2018, 2023) and ultra-stable (Stefansson et al. 2016; Robertson et al. 2019) NEID spectrograph has been operational since 2022, covering a wavelength range of 380 to 930 nm. Observations of these five targets were conducted on the following dates: UT June 14, 2023; October 17, 2023; April 6, 2023; March 20, 2024; and December 21, 2023, respectively, yielding a total of 88 measurements. Apart from the in-transit RVs, for TOI-3972, we collected 13 additional out-of-transit RVs from UT October 18, 2023 to January 29, 2024 using NEID. We also collected an additional six RVs for TOI-2025 on April 4, 2023, using NEID.

The NEID spectra were analyzed using version 1.3.0 of the NEID Data Reduction Pipeline (NEID-DRP)<sup>3</sup>. The DRP adopted the cross-correlation function (CCF) method to derive the radial velocities. Barycentric-corrected radial velocities for re-weighted orders (CCFRVMOD) were extracted from the NExScI NEID Archive<sup>4</sup>.

A comprehensive summary of the observations conducted by PFS and NEID is presented in Table 1. The resulting RVs, available through the Data behind the Figure program (see caption of Figure 1), are displayed in Figure 1.

## 3. PHOTOMETRY

The *TESS* data used in this analysis were reduced by the *TESS* Science Processing Operations Center (SPOC; Jenkins et al. 2016) at NASA Ames Research Center to obtain Presearch Data Conditioning simple aperture photometry (PDCSAP; Smith et al. 2012; Stumpe et al. 2012, 2014) light curves. Table 1 indicates the cadence at which data were acquired for each TOI and for each sector. The SPOC light curves were obtained at 2-min cadence and the *TESS*-SPOC light curves from Full Frame Images (FFIs; Caldwell et al. 2020). The transit signatures of TOIs 559 b, 2031 b,

<sup>3</sup> Detailed information available at <https://neid.ipac.caltech.edu/docs/NEID-DRP/>.

<sup>4</sup> Available at <https://neid.ipac.caltech.edu/>.

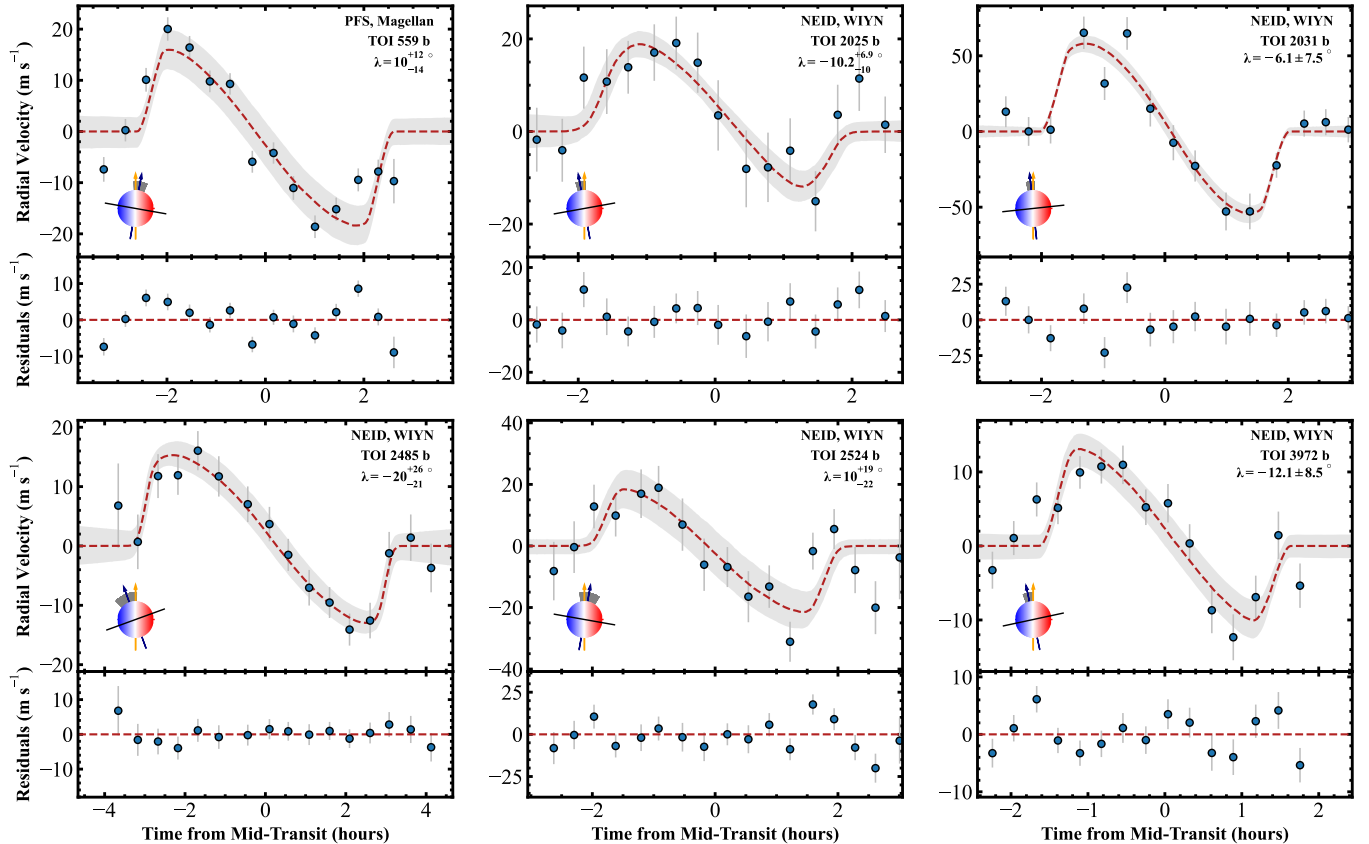


**Figure 1.** Rossiter-McLaughlin measurements for TOI-559 b, TOI-2025 b, TOI-2031 b, TOI-2485 b, TOI-2524 b and TOI-3972 b are shown as a function of hours from mid-transit. The RM data, with the Keplerian signal subtracted, are represented as blue dots. The median RM models are each depicted using red dashed lines. The  $1\sigma$  credible intervals are indicated by grey areas. In the lower-left corner, a schematic diagram illustrates the sky-projected stellar obliquity. Orange arrows indicate the projected stellar spin axis, while black arrows represent the planetary orbital axis, with its uncertainty shown in grey. Black lines illustrate the planetary orbital plane. Residuals are displayed beneath each panel. The RV data used in this work are available via this [link](#).

2485 b, and 3972 b were all initially detected by the *TESS* Quick Look Pipeline (QLP; [Huang et al. 2020a,b](#)) and alerted by the *TESS* project to the community ([Guerrero et al. 2021](#)). Note that *TESS* Year 2 sectors (14-26) are affected by a sky background bias which starting in Sector 27 was addressed by the algorithm documented in the associated *TESS* Data Release Note DR38<sup>5</sup>. We thus analyzed the target pixel and light curve files of the affected targets and sectors (TOI-2031, Sectors 18, 19, 24, 25, 26; TOI-3972, Sectors 17, 18, 24; and TOI-2485, Sector 23) to determine whether there was a significant effect in these cases. We found that the bias induced on the planetary radii for TOI-2031 ( $<1\%$ ) and TOI-2485 ( $\sim 0.3\%$ ) was small compared to the respective overall errors ( $\sim 3.2\%$  and  $\sim 5\%$ ; see Table 2). However, for TOI-3972 since this bias was higher, we

accounted for it in the fits, reducing the overall error on the planetary radius from  $\sim 3.4\%$  to  $\sim 2.4\%$  (see Table 2 for the latter). All *TESS* data used in this paper can be found in MAST: [10.17909/r8dh-5j34](#).

In this work, we also incorporated two new sets of ground-based photometry for TOI-2025 b and TOI-2031 b. Details on the observations and data reduction are provided in Appendix A.

## 4. STELLAR PARAMETERS

### 4.1. Synthetic spectral fitting by *iSpec*

Co-added NEID spectra and iodine-free PFS spectra were adopted to determine the star’s spectroscopic parameters, including stellar effective temperature ( $T_{\text{eff}}$ ), surface gravity ( $\log g_*$ ), metallicity ( $[\text{Fe}/\text{H}]$ ), and projected rotational velocity ( $v \sin i_*$ ). We used the synthetic spectral fitting technique provided by the Python package *iSpec* ([Blanco-Cuaresma et al. 2014](#); [Blanco-Cuaresma 2019](#)) to measure these parameters.

<sup>5</sup> [https://archive.stsci.edu/missions/tess/doc/tess\\_drn/tess\\_sector\\_27\\_drn38\\_v02.pdf](https://archive.stsci.edu/missions/tess/doc/tess_drn/tess_sector_27_drn38_v02.pdf)



We employed the SPECTRUM radiative transfer code (Gray & Corbally 1994), the MARCS atmosphere model (Gustafsson et al. 2008), and the sixth version of the GES atomic line list (Heiter et al. 2021), all incorporated within `iSpec`, to create a synthetic model for the iodine-imprinted PFS spectra and the co-added NEID spectra (S/N: TOI-559, 188; TOI-2025, 83; TOI-2031, 88; TOI-2485, 151; TOI-2524, 41; TOI-3972, 96). We treated micro-turbulent velocities as a variable in our fitting process, allowing us to accurately represent the small-scale turbulent motions in the stellar atmosphere. Macro-turbulent velocities were determined using an empirical relationship that leverages established correlations with various stellar attributes (Doyle et al. 2014). We selected specific spectral regions to streamline the fitting process, focusing on the wings of the  $H\alpha$ ,  $H\beta$ , and Mg I triplet lines, which are tracers of  $T_{\text{eff}}$  and  $\log g_*$ , as well as Fe I and Fe II lines that are crucial for constraining  $[\text{Fe}/\text{H}]$  and  $v \sin i_*$ . Spectroscopic parameters were refined using the Levenberg-Marquardt nonlinear least-squares fitting algorithm (Markwardt 2009), which iteratively minimizes the  $\chi^2$  value between the synthetic and observed spectra. The final spectroscopic parameters are detailed in Table 2.

#### 4.2. SED+MIST fit by EXOFASTv2

To derive additional stellar parameters, such as stellar mass ( $M_*$ ) and radius ( $R_*$ ), we utilized the MESA Isochrones & Stellar Tracks (MIST) model (Choi et al. 2016; Dotter 2016) in combination with a spectral energy distribution (SED) fitting approach. Photometry was compiled from various catalogs, including 2MASS (Cutri et al. 2003), WISE (Cutri et al. 2021), *TESS* (Ricker et al. 2015), and Gaia DR3 (Gaia Collaboration et al. 2023). Gaussian priors based on our synthetic spectral fitting were applied to  $T_{\text{eff}}$  and  $[\text{Fe}/\text{H}]$ , along with the parallax from Gaia DR3 and an upper limit for the  $V$ -band extinction from (Schlafly & Finkbeiner 2011)<sup>6</sup>. A 2.4% systematic uncertainty floor in  $T_{\text{eff}}$  was adopted, as suggested by Tayar et al. (2022).

The SED fitting was performed using the Differential Evolution Markov Chain Monte Carlo (DE-MCMC) technique, integrated within EXOFASTv2 (Eastman 2017; Eastman et al. 2019) to evaluate uncertainties. The MCMC procedure was considered converged when the Gelman-Rubin diagnostic ( $\hat{R}$ ; Gelman & Rubin 1992) fell below 1.01 and the count of independent draws surpassed 1000. The resulting stellar parameters are listed in Table 2.

## 5. OBLIQUITY MODELING

To derive the sky-projected spin-orbit angles, a modified version of `allesfitter` (Günther & Daylan 2021, 2019) was adopted to conduct simultaneous fits to transits, radial velocities, and Rossiter-McLaughlin measurements. The transit and radial velocity models were integrated using `PyTransit` (Parviainen 2015) and `RadVel` (Fulton et al. 2018), respectively. The RM model, grounded in Hirano et al. (2011), was implemented in `tracit` (Hjorth et al. 2021; Knudstrup & Albrecht 2022).

The RM, ground-based photometric, and *TESS* data included within our fits are listed in Table 1. We also incorporated out-of-transit RVs for TOI-559, TOI-2025, TOI-2524, and, TOI-3972. The RVs of TOI-559, as presented by Ikwut-Ukwa et al. (2022), were obtained using the 1.5m Tillinghast Reflector Echelle Spectrograph (TRES, Furész et al. 2008) on the 1.5m Tillinghast Reflector and CTIO High-Resolution spectrometer (CHIRON, Tokovinin et al. 2013) on the CTIO 1.5-meter telescope. The out-of-transit RVs for TOI-2025 include 16 from TRES, 6 from WIYN, and 39 from the Fiber-fed Echelle Spectrograph (FIES; Telting et al. 2014; Telting et al. 2014) on the Nordic Optical Telescope (NOT; Djupvik & Andersen 2010). For TOI-2025, we included an additional RM observation drawn from Knudstrup et al. (2022), which consists of 16 RVs from FIES from which Knudstrup et al. (2022) previously derived  $\lambda = 9_{-34}^{+36}$ °. For TOI-2524, an additional eight out-of-transit RVs from CHIRON were adopted. For TOI-3972, 13 additional out-of-transit RVs from NEID were also adopted.

We drew initial guesses for the orbital period ( $P$ ), the reference transit mid-time ( $T_0$ ), the cosine of the planet’s orbital inclination ( $\cos i$ ), the radius ratio of the planet to host ( $R_p/R_*$ ), the sum of the stellar and planetary radii divided by the semimajor axis ( $(R_* + R_p)/a$ ), and the radial velocity semi-amplitude ( $K$ ) from the values derived from the Exoplanet Follow-up Observing Program (ExoFOP) website<sup>7</sup>. All fitted parameters were allowed to vary and were initialized with uniform priors. For TOI-559, TOI-2025, TOI-2524, and TOI-3972, which each included out-of-transit RVs in their models, the two eccentricity parameters  $\sqrt{e} \sin \omega$  and  $\sqrt{e} \cos \omega$  were each initialized with a value of 0. Because no out-of-transit RVs were included within our models of TOI-2031 and TOI-2485, we fixed their eccentricities to zero. The two transformed quadratic limb-darkening co-

<sup>7</sup> <https://exofop.ipac.caltech.edu/tess/>

<sup>6</sup> <https://irsa.ipac.caltech.edu/applications/DUST/>

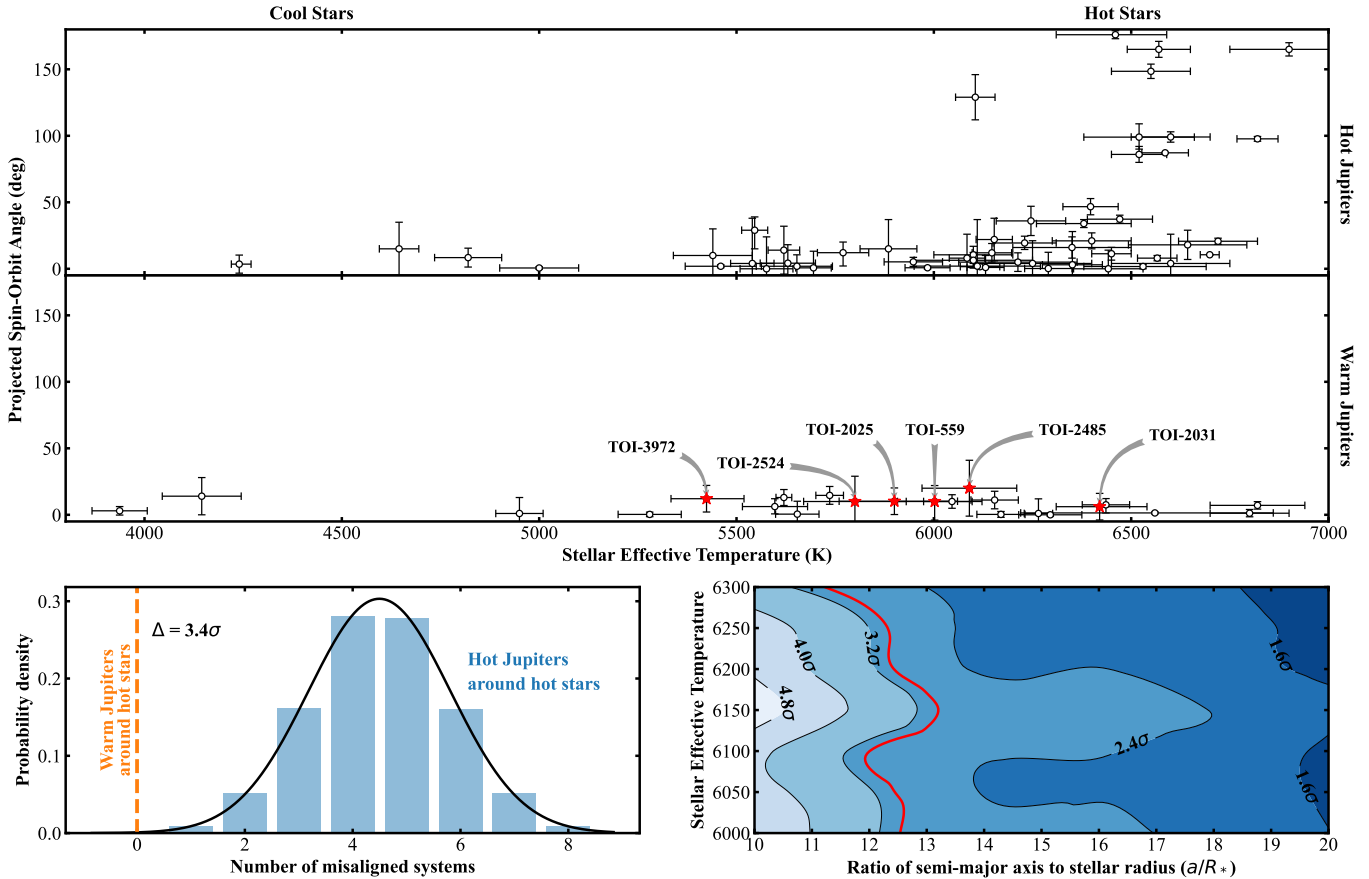


**Figure 2.** **Upper panel:** the distribution of sky-projected stellar obliquity ( $|\lambda|$ ) for Jovian planets around hot and cool stars as a function of stellar effective temperature. The obliquity measurements conducted by this work are shown as red stars. **Lower panel:** *Left:* The greater alignment of hot-star warm-Jupiter systems compared to hot-star hot-Jupiter systems is shown, with the number of misaligned systems for each type represented in orange and blue, respectively. The black line represents the fitted Gaussian function profile. *Right:* significance levels as a function of  $T_{\text{eff}}$  and  $a/R_*$ . The brighter regions have higher significance levels. Black lines indicate significance levels, with inline numbers showing the values. The 3 $\sigma$  significance level lines are shown in red. The dataset used to create this figure is available via this [link](#).

efficients  $q_1$  and  $q_2$ <sup>8</sup> for each in-transit dataset (including each photometric band and each instrument used for the RM observation) were initialized with a value of 0.5. Uniform priors ranging from 0 to 1 were applied to  $\cos i$ . The sky-projected spin-orbit angle  $\lambda$  was initialized with a value of  $0^\circ$  and allowed to vary between  $\pm 180^\circ$ . Furthermore, we incorporated Gaussian priors for macro-turbulence ( $\zeta$ ) and micro-turbulence ( $\xi$ ) to reflect stellar surface motion. These priors were from Doyle et al. (2014) for macro-turbulence and Jofré et al. (2014) for micro-turbulence, with a standard deviation of 1 km/s applied.

<sup>8</sup> The relations between the transformed ( $q_1$ ,  $q_2$ ) and physical ( $u_1$ ,  $u_2$ ) quadratic limb-darkening coefficients are defined by Equations 15 and 16 in Kipping (2013):  $u_1 = 2\sqrt{q_1}q_2$  and  $u_2 = \sqrt{q_1}(1 - 2q_2)$ .

The *TESS* light curves were detrended using Gaussian Processes with a Matern 3/2 kernel, implemented in *wotan* (Hippke et al. 2019). For each ground-based transit, a third-order polynomial function was employed to model potential trends. To accommodate the RV offset in the out-of-transit RVs, both a constant baseline and a jitter term were incorporated. For each RM fit, a polynomial was utilized to address short-term overnight instrumental systematics and stellar variability. To determine the optimal degree of the polynomial, we conducted RM-only fits in which only the  $v \sin i_*$ ,  $\lambda$ , and polynomial parameters were allowed to vary, with polynomial degrees ranging from 0 to 3. The best fits were obtained through global optimization using differential evolution, implemented in *PyDE* (Storn & Price 1997). The polynomial yielding the lowest Bayesian Information Criterion was ultimately selected. Furthermore, to account for potential distortions caused by the long ex-

posure times ( $>1000$  s) of our RM observations, we performed exposure interpolation during the fitting process to produce 2-minute sampling for each RM fit.

To sample the posterior distributions of all fitted parameters, we employed the affine-invariant Markov Chain Monte Carlo (MCMC) method as implemented in the `emcee` (Foreman-Mackey et al. 2013) Python package, using 100 walkers. The total number of accepted steps exceeded 200,000, and we discarded the initial 20% of these steps as burn-in. The chains were deemed to have converged only if all chains were longer than 50 times their autocorrelation lengths. The derived parameters are tabulated in Table 2.

For all six targets, we applied the autocorrelation function as implemented in `SpinSpotter` (Holcomb et al. 2022) and the Generalized Lomb-Scargle periodogram (Zechmeister & Kürster 2009) to the *TESS* light curve. This process did not yield a confident identification of the rotation period in any of the six systems, preventing us from establishing limits on their true obliquity.

## 6. STATISTICAL ANALYSIS

In the past several years, the number of warm Jupiters with Rossiter-McLaughlin measurements has increased significantly (e.g., Kepler-448 b/KOI-12 b, Bourrier et al. 2015; Johnson et al. 2017; K2-140 b, Rice et al. 2021; K2-232 b, Wang et al. 2021; Qatar-6 b, Rice et al. 2023a; TOI-1478 b, Rice et al. 2022b; TOI-1670 c, Lubin et al. 2023; TOI-1859 b, Dong et al. 2023; TOI-2202 b, Rice et al. 2023b; TOI-677 b, Sedaghati et al. 2023; Hu et al. 2024; TOI-3362 b, Espinoza-Retamal et al. 2023; TOI-4201 b, Gan et al. 2024; TOI-4641 b, Bieryla et al. 2024; and WASP-106 b, Wright et al. 2023; Harre et al. 2023; Prinoth et al. 2024). By combining newly collected RM data with literature RMs and following the procedure described in Appendix B, we obtained a sample of 78 Jovian-planet systems without known stellar companions. This includes 55 hot-Jupiter systems and 23 warm-Jupiter systems, providing a valuable opportunity to explore the connection between stellar obliquity and the dynamical histories of warm Jupiters. Notably, to date, SOLES has contributed 14 of these 23 RM measurements to the warm-Jupiter sample.

### 6.1. Statistical Significance of the Aligned Single-Star Warm-Jupiter System Trend

We subsequently utilized this sample to examine whether warm-Jupiter and hot-Jupiter systems exhibit similar or distinct misalignment distributions. In this

work, we define a “misaligned” system as one in which the angle  $|\lambda|$  exceeds  $10^\circ$  and differs from  $0^\circ$  at the  $3\sigma$  level (Wang et al. 2022; Rice et al. 2022b). All other systems are considered “aligned”.

Previous studies have shown that hot-Jupiter systems are often misaligned in the presence of host stars with high stellar effective temperatures (above the Kraft break,  $T_{\text{eff}} \approx 6100$  K, Kraft 1967). However, due to a previously small sample size, it has so far been unclear whether this host star temperature trend extends to warm-Jupiter systems. The larger, clean sample of hot- and warm-Jupiter systems constructed within this work provides the necessary context for a comparative study examining the dependence of stellar obliquities on host star temperature.

#### *Single-cool-star systems with giants tend to be aligned:*

In systems with cool stars ( $T_{\text{eff}} < 6100$  K), there are 19 hot-Jupiter systems and 14 warm-Jupiter systems with RM measurements, all of which are aligned. Consequently, to date, no robust observational evidence suggests that Jupiters around single cool stars can be spin-orbit misaligned.

To compare if the projected stellar obliquity distributions of cool-star hot-Jupiter and cool-star warm-Jupiter systems are identical, we applied the Kolmogorov-Smirnov (K-S, Hodges 1958) and Anderson-Darling (A-D, Scholz & Stephens 1987) tests, implemented in `scipy` (Virtanen et al. 2020). The null hypothesis is that these distributions are the same. We resampled the  $|\lambda|$  values with associated uncertainties and conducted 10,000 trials to derive the distribution of the p-values for the K-S and A-D tests. To be conservative, we adopted the larger value between the lower and upper uncertainties for each  $|\lambda|$ . The resulting distribution of p-values for the K-S and A-D tests showed that merely 4.3% and 1.6% of the values, respectively, fell below the 0.05 threshold, failing to reject the null hypothesis. This indicates that the alignment tendency of cool-star hot-Jupiter systems are similar to those of cool-star warm-Jupiter systems.

#### *Single-hot-star warm-Jupiter systems tend to be aligned:*

Our sample includes 36 hot Jupiters and 9 warm Jupiters around hot stars ( $T_{\text{eff}} \geq 6100$  K), with all of these warm Jupiters exhibiting spin-orbit alignment. To determine the misalignment probability in hot-Jupiter systems, we iteratively draw random samples of 9  $|\lambda|$  values from the hot-star hot-Jupiter sample without replacement to see how many of them are misaligned. This process was repeated until the distribution of the number of misaligned systems stabilized, which occurred after 100,000 iterations. Since all nine warm Jupiters around hot stars are aligned, we found a  $3.4\text{--}\sigma$  differ-



Table 2. Stellar and Planetary Parameters

	TOI-559	TOI-2025	TOI-2031	TOI-2485	TOI-2524	TOI-3972
<b>Stellar Coordinates and Magnitudes:</b>						
TIC id	209459275	394050135	470127886	328934463	169249234	284206913
Gaia DR3	5057924844082070016	2296342614570999552	2299101254886404608	1443530266145475840	3802583419029393152	427232186629403264
V	11.091 ± 0.007	11.599 ± 0.021	11.254 ± 0.010	11.935 ± 0.026	12.800 ± 0.103	11.349 ± 0.017
<b>Stellar Parameters:</b>						
Synthetic spectral fit:						
$T_{\text{eff}}$	6037.08 ± 121.53	6086.83 ± 80.21	6415.2 ± 105.59	6137.43 ± 96.49	5866.50 ± 102.60	5420.42 ± 70.59
[Fe/H]	-0.27 ± 0.07	0.12 ± 0.05	-0.21 ± 0.07	0.1 ± 0.06	0.14 ± 0.06	0.21 ± 0.05
log $g_*$	4.45 ± 0.18	4.31 ± 0.16	4.44 ± 0.22	4.2 ± 0.17	4.52 ± 0.13	4.62 ± 0.15
$v \sin i_*$	3.74 ± 0.66	3.98 ± 0.60	4.66 ± 0.91	4.39 ± 0.62	2.44 ± 0.56	2.22 ± 0.38
SED+MIST fit (adopted):						
$M_*$	0.976 <sup>+0.067</sup> <sub>-0.059</sub>	1.129 <sup>+0.12</sup> <sub>-0.088</sub>	1.103 ± 0.073	1.262 <sup>+0.084</sup> <sub>-0.12</sub>	1.022 <sup>+0.066</sup> <sub>-0.059</sub>	0.927 <sup>+0.047</sup> <sub>-0.037</sub>
$R_*$	1.235 <sup>+0.041</sup> <sub>-0.040</sub>	1.524 <sup>+0.014</sup> <sub>-0.015</sub>	1.238 <sup>+0.040</sup> <sub>-0.038</sub>	1.682 <sup>+0.066</sup> <sub>-0.060</sub>	1.131 <sup>+0.016</sup> <sub>-0.014</sub>	0.945 <sup>+0.029</sup> <sub>-0.028</sub>
$T_{\text{eff}}$	6002 <sup>+95</sup> <sub>-94</sub>	5900 <sup>+160</sup> <sub>-140</sub>	6420 <sup>+120</sup> <sub>-110</sub>	6090 ± 120	5800 ± 130	5424 <sup>+95</sup> <sub>-90</sub>
[Fe/H]	-0.199 <sup>+0.077</sup> <sub>-0.11</sub>	0.13 ± 0.13	-0.197 <sup>+0.064</sup> <sub>-0.082</sub>	0.094 <sup>+0.058</sup> <sub>-0.060</sub>	0.136 <sup>+0.076</sup> <sub>-0.080</sub>	0.214 <sup>+0.048</sup> <sub>-0.050</sub>
log $g_*$	4.244 <sup>+0.045</sup> <sub>-0.043</sub>	4.130 <sup>+0.058</sup> <sub>-0.065</sub>	4.295 <sup>+0.040</sup> <sub>-0.042</sub>	4.085 <sup>+0.042</sup> <sub>-0.054</sub>	4.330 ± 0.049	4.455 <sup>+0.032</sup> <sub>-0.031</sub>
Age	8.2 <sup>+3.0</sup> <sub>-2.7</sub>	6.4 <sup>+2.9</sup> <sub>-2.6</sub>	3.7 <sup>+2.3</sup> <sub>-1.8</sub>	4.1 <sup>+2.4</sup> <sub>-1.2</sub>	7.3 <sup>+3.4</sup> <sub>-3.5</sub>	8.4 <sup>+3.4</sup> <sub>-3.8</sub>
$\varpi$	4.317 ± 0.019	2.930 <sup>+0.017</sup> <sub>-0.016</sub>	3.619 ± 0.016	2.527 ± 0.056	2.315 <sup>+0.020</sup> <sub>-0.021</sub>	6.132 ± 0.017
d	231.62 <sup>+1.0</sup> <sub>-0.99</sub>	341.3 <sup>+1.9</sup> <sub>-2.0</sub>	276.3 <sup>+1.3</sup> <sub>-1.2</sub>	395.7 <sup>+9.0</sup> <sub>-8.5</sub>	432.0 <sup>+4.5</sup> <sub>-3.6</sub>	163.09 <sup>+0.45</sup> <sub>-0.44</sub>
<b>Rossiter-McLaughlin Parameters:</b>						
$\lambda$	10 <sup>+12</sup> <sub>-14</sub>	-10.2 <sup>+6.9</sup> <sub>-10.0</sub>	-6.1 ± 7.5	-20 <sup>+26</sup> <sub>-21</sub>	10 <sup>+19</sup> <sub>-22</sub>	-12.1 ± 8.5
$v \sin i_*$	2.93 ± 0.38	5.43 <sup>+0.99</sup> <sub>-0.93</sub>	6.56 ± 0.60	4.26 <sup>+0.96</sup> <sub>-0.69</sub>	2.38 <sup>+0.57</sup> <sub>-0.62</sub>	1.20 ± 0.16
$\xi$	1.26 <sup>+0.93</sup> <sub>-0.76</sub>	1.29 <sup>+0.89</sup> <sub>-0.77</sub>	1.27 <sup>+0.92</sup> <sub>-0.76</sub>	1.48 <sup>+0.94</sup> <sub>-0.83</sub>	1.27 <sup>+0.91</sup> <sub>-0.77</sub>	1.18 <sup>+0.88</sup> <sub>-0.73</sub>
$\zeta$	3.90 ± 1.0	4.68 ± 0.95	5.44 ± 0.99	4.68 ± 0.99	3.40 ± 1.0	2.11 ± 0.99
<b>Planetary Parameters:</b>						
$\frac{R_b}{R_*}$	0.09211 <sup>+0.00088</sup> <sub>-0.00095</sub>	0.07604 <sup>+0.00098</sup> <sub>-0.0010</sub>	0.10557 ± 0.00061	0.0682 ± 0.0022	0.1016 <sup>+0.0017</sup> <sub>-0.0028</sub>	0.12564 <sup>+0.00042</sup> <sub>-0.00049</sub>
$\frac{(R_* + R_b)}{a_b}$	0.0933 ± 0.0026	0.1318 <sup>+0.0043</sup> <sub>-0.0052</sub>	0.0989 ± 0.0015	0.0782 <sup>+0.0037</sup> <sub>-0.0024</sub>	0.0787 <sup>+0.0020</sup> <sub>-0.0019</sub>	0.05260 ± 0.00047
cos $i_b$	0.0340 <sup>+0.0042</sup> <sub>-0.0049</sub>	0.172 <sup>+0.021</sup> <sub>-0.028</sub>	0.0362 <sup>+0.0035</sup> <sub>-0.0038</sub>	0.020 <sup>+0.011</sup> <sub>-0.012</sub>	0.0333 <sup>+0.0043</sup> <sub>-0.011</sub>	0.03093 ± 0.00064
$T_{0,b}$	9312.84866 ± 0.00067	9400.05721 ± 0.00066	9634.56512 ± 0.00010	9490.2896 ± 0.0029	9469.94454 ± 0.00050	9356.64809 ± 0.00079
$P_b$	6.9839122 ± 0.0000070	8.872079 <sup>+0.000010</sup> <sub>-0.000011</sub>	5.7154834 ± 0.0000020	11.234813 ± 0.000061	7.1858163 ± 0.0000063	10.511372 ± 0.000015
$K_b$	0.6374 ± 0.0063	0.375 ± 0.018	0.057 <sup>+0.031</sup> <sub>-0.029</sub>	0.205 ± 0.029	0.0674 ± 0.0045	0.521 ± 0.025
$\sqrt{e_b} \cos \omega_b$	0.181 ± 0.010	-0.039 ± 0.077	0.0 (fixed)	0.0 (fixed)	-0.02 <sup>+0.15</sup> <sub>-0.15</sub>	-0.193 ± 0.011
$\sqrt{e_b} \sin \omega_b$	-0.346 ± 0.016	0.670 <sup>+0.013</sup> <sub>-0.015</sub>	0.0 (fixed)	0.0 (fixed)	-0.137 <sup>+0.084</sup> <sub>-0.066</sub>	0.4802 <sup>+0.0078</sup> <sub>-0.010</sub>
$q_{1,\text{FPS}}$	0.50 ± 0.34	-	-	-	-	-
$q_{2,\text{FPS}}$	0.42 <sup>+0.36</sup> <sub>-0.27</sub>	-	-	-	-	-
$q_{1,\text{NEID}}$	-	0.56 <sup>+0.30</sup> <sub>-0.34</sub>	0.55 <sup>+0.31</sup> <sub>-0.34</sub>	0.57 <sup>+0.30</sup> <sub>-0.35</sub>	0.58 <sup>+0.29</sup> <sub>-0.35</sub>	0.60 <sup>+0.29</sup> <sub>-0.35</sub>
$q_{2,\text{NEID}}$	-	0.48 <sup>+0.31</sup> <sub>-0.27</sub>	0.51 ± 0.31	0.50 <sup>+0.30</sup> <sub>-0.28</sub>	0.53 ± 0.30	0.52 <sup>+0.31</sup> <sub>-0.29</sub>
$q_{1,\text{FIES}}$	-	0.50 ± 0.34	-	-	-	-
$q_{2,\text{FIES}}$	-	0.55 <sup>+0.31</sup> <sub>-0.38</sub>	-	-	-	-
<b>Derived Parameters:</b>						
$M_b$	7.13 ± 0.53	5.46 <sup>+0.37</sup> <sub>-0.41</sub>	-	-	0.648 <sup>+0.064</sup> <sub>-0.060</sub>	3.67 ± 0.23
$R_b$	1.085 ± 0.031	1.127 ± 0.019	1.272 ± 0.041	1.116 ± 0.056	1.116 <sup>+0.025</sup> <sub>-0.032</sub>	1.126 ± 0.027
$\frac{a_b}{R_*}$	11.71 <sup>+0.33</sup> <sub>-0.31</sub>	13.17 <sup>+0.34</sup> <sub>-0.26</sub>	11.17 ± 0.17	13.65 <sup>+0.43</sup> <sub>-0.61</sub>	13.99 ± 0.35	21.40 ± 0.19
$a_b$	0.0659 ± 0.0026	0.0579 <sup>+0.0025</sup> <sub>-0.0019</sub>	0.0644 ± 0.0022	0.1064 <sup>+0.0055</sup> <sub>-0.0050</sub>	0.0736 ± 0.0021	0.0917 ± 0.0023
$i_b$	88.05 <sup>+0.28</sup> <sub>-0.24</sub>	80.1 <sup>+1.7</sup> <sub>-1.2</sub>	87.93 <sup>+0.22</sup> <sub>-0.20</sub>	88.86 <sup>+0.70</sup> <sub>-0.65</sub>	88.09 <sup>+0.66</sup> <sub>-0.25</sub>	88.228 ± 0.037
$e_b$	0.1521 ± 0.0092	0.455 ± 0.017	-	-	0.036 <sup>+0.036</sup> <sub>-0.023</sub>	0.2680 <sup>+0.0063</sup> <sub>-0.0072</sub>
$\omega_b$	297.6 <sup>+2.2</sup> <sub>-2.1</sub>	93.3 ± 6.6	-	-	259 <sup>+59</sup> <sub>-45</sub>	112.0 <sup>+1.4</sup> <sub>-1.3</sub>
$T_{14;b}$	5.193 <sup>+0.033</sup> <sub>-0.031</sub>	3.91 <sup>+0.31</sup> <sub>-0.25</sub>	4.029 ± 0.013	6.491 <sup>+0.11</sup> <sub>-0.094</sub>	4.016 <sup>+0.16</sup> <sub>-0.079</sub>	3.420 ± 0.013
$T_{23;b}$	4.113 <sup>+0.049</sup> <sub>-0.045</sub>	2.67 <sup>+0.52</sup> <sub>-0.46</sub>	3.122 ± 0.029	5.58 ± 0.12	3.06 <sup>+0.29</sup> <sub>-0.12</sub>	2.146 ± 0.021

Note :

$T_{\text{eff}}$ : effective temperature (K), [Fe/H]: metallicity (dex), log  $g_*$ : surface gravity ( $\log_{10}(\text{cm/s}^2)$ ),  $v \sin i_*$ : projected stellar rotational velocity (km/s),  $M_*$ : stellar mass ( $M_{\odot}$ ),  $R_*$ : stellar radius ( $R_{\odot}$ ),  $T_{\text{eff}}$ : effective temperature (K), [Fe/H]: metallicity (dex), log  $g_*$ : surface gravity ( $\log_{10}(\text{cm/s}^2)$ ), Age: age (Gyr),  $\varpi$ : parallax (mas), d: distance (pc),  $\lambda$ : sky-projected spin-orbit angle (deg),  $v \sin i_*$ : projected stellar rotational velocity (km/s),  $\xi$ : micro-turbulent velocity (km/s),  $\zeta$ : macro-turbulent velocity (km/s),  $R_b/R_*$ : planet-to-star radius ratio,  $(R_* + R_b)/a_b$ : ratio of the sum of star and planet radii to semi-major axis, cos  $i_b$ : cosine of inclination,  $T_{0,b}$ : mid-transit time - 2450000 (BJD<sub>TDB</sub>),  $P_b$ : orbital period (days),  $K_b$ : radial velocity semi-amplitude (m/s),  $\sqrt{e_b} \cos \omega_b$  and  $\sqrt{e_b} \sin \omega_b$ : eccentricity vector components,  $q_1$  and  $q_2$ : transformed limb-darkening coefficients,  $M_b$ : planetary mass ( $M_{\text{Jup}}$ ),  $R_b$ : planetary radius ( $R_{\text{Jup}}$ ),  $a_b/R_*$ : semi-major axis scaled by stellar radius,  $a_b$ : semi-major axis (AU),  $i_b$ : inclination (deg),  $e_b$ : eccentricity,  $\omega_b$ : argument of periastron,  $T_{14;b}$ : total transit duration (hours),  $T_{23;b}$ : full transit duration (hours).

ence between the hot-star hot-Jupiter systems and the hot-star warm-Jupiter systems, as shown in the lower left panel of Figure 2. Furthermore, we examine the dependency of statistical significance on the choice of the difference criteria, varying  $a/R_*$  from 10 to 20 and  $T_{\text{eff}}$  from 6100 to 6300 K (see the lower right panel of Figure 2). For 98% of the area where  $6000 \leq T_{\text{eff}} \leq 6300$  K and  $10 \leq a/R_* \leq 12$ , the significance level is  $\geq 3\sigma$ . A more straightforward approach to verify this result is as follows: among 36 hot-star hot-Jupiter systems, 18 are misaligned, corresponding to a misalignment rate of 50%. The probability of randomly drawing nine systems and finding that all are aligned is  $0.50^9 \approx 0.2\%$ , indicating a  $3.1\text{-}\sigma$  occurrence.

Additionally, we treat hot-Jupiter and warm-Jupiter systems as two groups without distinguishing between aligned and misaligned. We applied the K-S and A-D tests utilizing the aforementioned approach to study whether the projected stellar obliquity distribution of hot-star hot-Jupiter and hot-star warm-Jupiter systems is identical. The null hypothesis is that they are identical. The analysis of the p-value distributions demonstrated that 70% of the p-values from the K-S test and 85% of the p-values from the A-D test fell below the 0.05 threshold, allowing us to reject the null hypothesis and highlighting the significant disparity between the two samples.

## 7. THEORETICAL IMPLICATIONS

In our analysis of Rossiter-McLaughlin measurements, we identified a  $3.4\text{-}\sigma$  trend<sup>9</sup>: single-star warm-Jupiter systems consistently exhibit no spin-orbit misalignments, even above the Kraft break, demonstrating a  $3.4\text{-}\sigma$  confidence difference when compared to the  $T_{\text{eff}}\text{-}\lambda$  dependency found in hot-Jupiter systems. This trend presents intriguing contrasts with the orbital orientations of hot Jupiters, which typically align with cooler stars but often show misalignment around hotter ones.

One explanation for these contrasting alignment trends is that hot and warm Jupiters might originate from different formation processes. Warm Jupiters could form directly from well-aligned protoplanetary disks, leading to an initial alignment (albeit with some low-level,  $\lesssim 20^\circ$  range of expected primordial misalignments; see Rice et al. 2023b). This interpretation is in agreement with findings from Morgan et al. (2024), which found that giant planets around cool stars out to  $\sim 2$  AU

are preferentially aligned. It is also supported by a growing body of evidence for primordial alignment from direct imaging observations of giant planets around young stars (Kraus et al. 2020; Bowler et al. 2023; Franson et al. 2023; Sepulveda et al. 2024) and from both protoplanetary (Davies 2019) and debris disk (Hurt & MacGregor 2023) spin-orbit constraints. By contrast, hot Jupiters, irrespective of stellar host temperature, may emerge from more violent evolutionary processes – often associated with high-eccentricity migration – after protoplanetary disk dispersal, resulting in initial misalignment. Subsequently, only cooler stars with hot Jupiters undergo tidal realignment, shaping the observed obliquity distribution in hot-Jupiter systems (Albrecht et al. 2012; Rice et al. 2022a; Zanazzi et al. 2024).

The observed sharp transitions near the Kraft break in the relationship between a star’s effective temperature and the alignment of hot Jupiter orbits strongly support tidal realignment mechanisms. However, these observations do not preclude the possibility that hot Jupiters around both cool and hot stars might initially have different obliquity distributions. Hot Jupiters around cooler stars, which may have formed and evolved quiescently, tend to be aligned (Wu et al. 2023; Hixenbaugh et al. 2023). By contrast, hot Jupiters around hot stars may often experience violent formation histories that lead to significant spin-orbit misalignments (Wu et al. 2023).

This scenario may arise if, for example, higher-mass stellar hosts preferentially form multiple Jupiter-mass planets. Following the dispersal of the protoplanetary disk, planet-planet interactions would naturally increase eccentricities and excite spin-orbit misalignments. As these orbits circularize, the initially eccentric and misaligned warm and cold Jupiters evolve into misaligned hot Jupiters around hotter stars. This explanation also accounts for why current observations show warm Jupiters around hot stars as aligned.

The fundamental factor here is the relative ease of exciting eccentricities over inducing inclinations (Petrovich 2015b; Espinoza-Retamal et al. 2023; Sedaghati et al. 2023), suggesting that warm Jupiters with significant initial misalignments likely underwent high eccentricities that drove their inward migration, transforming them into misaligned hot Jupiters. The persistent misalignment in resulting hot Jupiters, even though their orbital eccentricity has been damped, can primarily be attributed to differences in tidal damping timescales between orbital circularization and spin-orbit realignment. The timescale for circularization, dominated by tides raised by the star on the planet, is typically much shorter than the timescale for realignment, driven by

<sup>9</sup> Two more anticipated RM measurements for hot-star warm-Jupiter systems from Espinoza-Retamal et al. (2024, in prep) and Knudstrup et al. (2024, in revision) will increase the significance level to  $3.9\sigma$ .

tides the planet induces on the star (Hut 1981; Ogilvie & Lin 2007). This disparity in timescales between damping eccentricity and realigning the host star effectively maintains the observed spin-orbit misalignment in these tidally circularized resulting hot Jupiters.

#### ACKNOWLEDGMENTS

We appreciate the valuable comments from our anonymous reviewer, which have significantly improved this manuscript. We thank Simon Albrecht, Emil Knudstrup, and Cristobal Petrovich for insightful discussions. We acknowledge support from the NASA Exoplanets Research Program NNH23ZDA001N-XRP (Grant No. 80NSSC24K0153). Additionally, M.R. and S.W. acknowledge support from the Heising-Simons Foundation, with M.R. supported by Grant #2023-4478, and S.W. supported by Grant #2023-4050. This research was supported in part by Lilly Endowment, Inc., through its support for the Indiana University Pervasive Technology Institute. The work of HPO has been carried out within the framework of the NCCR Planets supported by the Swiss National Science Foundation under grants 51NF40\_182901 and 51NF40\_205606. DR was supported by NASA under award number NNA16BD14C for NASA Academic Mission Services. This paper contains data taken with the NEID instrument, which was funded by the NASA-NSF Exoplanet Observational Research (NN-EXPLORE) partnership and built by Pennsylvania State University. NEID is installed on the WIYN telescope, which is operated by the National Optical Astronomy Observatory, and the NEID archive is operated by the NASA Exoplanet Science Institute at the California Institute of Technology. NN-EXPLORE is managed by the Jet Propulsion Laboratory, California Institute of Technology under contract with the National Aeronautics and Space Administration. Resources supporting this work were provided by the NASA High-End Computing (HEC) Program through the NASA Advanced Supercomputing (NAS) Division at Ames Research Center for the production of the SPOC data products. Funding for the TESS mission is provided by NASA's Science Mission Directorate. We acknowledge the use of public TESS data from pipelines at the TESS Science Office and at the TESS Science Processing Operations Center. This research has made use of the Exoplanet Follow-up Observation Program website, which is operated by the California Institute of Technology, under contract with the National Aeronautics and Space Administration under the Exoplanet Exploration Program. This paper includes data collected by the TESS mission that are publicly available from the Mikulski Archive for Space Telescopes (MAST). KAC

and CNW acknowledge support from the TESS mission via subaward s3449 from MIT. This work makes use of observations from the LCOGT network. Part of the LCOGT telescope time was granted by NOIRLab through the Mid-Scale Innovations Program (MSIP). MSIP is funded by NSF. This paper is based on observations made with the Las Cumbres Observatory's education network telescopes that were upgraded through generous support from the Gordon and Betty Moore Foundation. This research has made use of the Exoplanet Follow-up Observation Program (ExoFOP; DOI: 10.26134/ExoFOP5) website, which is operated by the California Institute of Technology, under contract with the National Aeronautics and Space Administration under the Exoplanet Exploration Program.

*Facilities:* WIYN/NEID, PFS/Magellan, LCOGT

*Software:* `allesfitter` (Günther & Daylan 2021, 2019), `AstroImageJ` (Collins et al. 2017), `emcee` (Foreman-Mackey et al. 2013), `EXOFASTv2` (Eastman 2017; Eastman et al. 2019), `iSpec` (Blanco-Cuaresma et al. 2014; Blanco-Cuaresma 2019), `matplotlib`

(Hunter 2007), `numpy` (Oliphant 2006; Walt et al. 2011; Harris et al. 2020), `pandas` (McKinney 2010), `PyDE` (Storn & Price 1997), `PyTransit` (Parviainen 2015), `scipy` (Virtanen et al. 2020), `TAPIR` (Jensen 2013a), `wotan` (Hippke et al. 2019).

## APPENDIX

### A. GROUND-BASED PHOTOMETRY

To measure the transit times near the epoch of our spectroscopic time series observations, we acquired ground-based time-series photometry of the fields around TOI-2025 and TOI-2031 as part of the *TESS* Follow-up Observing Program (TFOP; Collins 2019)<sup>10</sup>. We used the *TESS* Transit Finder, which is a customized version of the *Tapir* software package (Jensen 2013b), to schedule our transit observations.

#### A.1. TOI-2025

We observed a full transit window of TOI-2025 b in Pan-STARRS *z*-short band on UT 2023 June 14 from the Las Cumbres Observatory Global Telescope (LCOGT, Brown et al. 2013) 1 m network node at McDonald Observatory near Fort Davis, Texas, United States. The 1 m telescope is equipped with a  $4096 \times 4096$  SINISTRO camera having an image scale of  $0''.389$  per pixel, resulting in a  $26' \times 26'$  field of view. The images were calibrated by the standard LCOGT BANZAI pipeline (McCully et al. 2018), and differential photometric data were extracted using `AstroImageJ` (Collins et al. 2017). We used circular photometric apertures with radius  $4''.3$ . The target star aperture excluded all of the flux from the nearest known neighbor in the Gaia DR3 catalog (Gaia DR3 2296342644635200512), which is  $\sim 80''$  north of TOI-2025. The light curve data are available on the EXOFOP-TESS website<sup>11</sup> and are included in the global modeling described in Section 5.

#### A.2. TOI-2031

We observed a full transit window of TOI-2031.01 in Sloan *i'* band on UT 2023 July 06 from the LCOGT 1 m network node at McDonald Observatory. The images were calibrated by the standard LCOGT BANZAI pipeline, and differential photometric data were extracted using `AstroImageJ`. We used circular photometric apertures with radius  $6''.6$ . The target star aperture excluded all of the flux from the nearest known neighbor in the Gaia DR3 catalog (Gaia DR3 2296342644635200512), which is  $\sim 45''$  southwest of TOI-2031. The light curve data are available on the EXOFOP-TESS website<sup>12</sup> and are included in the global modeling described in Section 5.

### B. SAMPLE CONSTRUCTION

We began with the set of systems listed in the TEPcat orbital obliquity catalog<sup>13</sup> (Southworth 2011) as of July 25, 2024. We adopted the preferred values for  $\lambda$  and  $T_{\text{eff}}$  from the TEPcat catalog for each system. Other parameters were drawn from the Planetary Systems Composite Data table of the NASA Exoplanet Archive<sup>14</sup>. Note that the parameters for WASP-109 and WASP-111 were from Anderson et al. (2014). We followed the steps outlined below to define our sample.

1. *Minimize biases introduced by nonuniform measurement techniques.* We only included results derived from Rossiter-McLaughlin and Doppler tomography measurements to avoid the biases caused by other methods. For example, spot-crossing is particularly sensitive to systems that are either aligned or anti-aligned, whereas gravity darkening is most sensitive to misaligned systems (Siegel et al. 2023; Dong & Foreman-Mackey 2023; see Albrecht et al. 2022 for a review of stellar obliquity measurement methods). When selecting stellar obliquity measurements,

<sup>10</sup> <https://tess.mit.edu/followup>

<sup>11</sup> <https://exofop.ipac.caltech.edu/tess/target.php?id=394050135>

<sup>12</sup> <https://exofop.ipac.caltech.edu/tess/target.php?id=470127886>

<sup>13</sup> <https://www.astro.keele.ac.uk/jkt/tepcat/obliquity.html>

<sup>14</sup> <https://exoplanetarchive.ipac.caltech.edu/cgi-bin/TblView/nph-tblView?app=ExoTbIs&config=PSCompPars>

we prioritize the most recent results, with Rossiter-McLaughlin measurements receiving higher precedence than Doppler tomography measurements.

2. *Remove low-quality and contested measurements.* We removed the systems with low-quality or contested measurements as suggested by Albrecht et al. (2022), including CoRoT-1 (Bouchy et al. 2008; Pont et al. 2010), CoRoT-19 (Guenther et al. 2012), HATS-14 (Zhou et al. 2015), HAT-P-27 (Brown et al. 2012), WASP-1 (Simpson et al. 2011; Albrecht et al. 2011), WASP-2 (TriAUD et al. 2010; Albrecht et al. 2011), WASP-23 (TriAUD et al. 2011), WASP-49 (Wyttenbach et al. 2017), and WASP-134 (Anderson et al. 2018). Note that we also excluded HAT-P-17 considering the disagreement between its two measurements (Fulton et al. 2013,  $19_{-16}^{+14}$  °; Mancini et al. 2022,  $-27.5 \pm 6.7$ °)
3. *Remove binary and multi-star systems.* Apart from the relatively confined gravitational interactions within a single-star system, stellar obliquity can also be strongly influenced by stellar companions (e.g., Wu & Murray 2003; Fabrycky & Tremaine 2007; Naoz et al. 2012; Naoz 2016). Therefore, in this work, we have excluded stars with bound companions identified in *Gaia* DR3. Following the methods described in El-Badry et al. (2021) and Rice et al. (2022b), we checked for bound companions to each system, determining whether candidate companions meet the following criteria: 1) their proper motion is within 5 km/s of the planet-hosting star, and 2) their parallax is consistent with that of the planet-hosting star within  $5\sigma$ . Candidates satisfying both criteria were identified as stellar companions and subsequently removed from our sample. Moreover, systems listed in the Binary and Multiple Star systems catalog<sup>15</sup>(Schwarz et al. 2016), the catalog of Exoplanets in Visual Binaries (Fontanive & Bardalez Gagliuffi 2021), or flagged as having more than one star in NASA Exoplanet Archive were also excluded.
4. *Remove systems with the  $T_{\text{eff}}$  of host stars  $< 3500$  K or  $> 7000$  K.* To ensure uniformity in the effective temperature ( $T_{\text{eff}}$ ) range across both warm- and hot-Jupiter systems, exclusion criteria were applied where  $T_{\text{eff}}$  exceeds 7000 K or falls below 3500 K.

This procedure yielded 78 Jovian planets ( $M_{\text{pl}} \geq 0.3 M_{\text{J}}$ ) around single-star systems with stellar obliquity measurements, including 55 hot-Jupiter systems ( $a/R_* < 11$ ) and 23 warm-Jupiter systems ( $a/R_* \geq 11$ ). A  $0.1 M_{\text{J}}$  uncertainty was assumed for planetary measurements with only upper-limit values.

## REFERENCES

- Albrecht, S., Winn, J. N., Johnson, J. A., et al. 2011, ApJ, 738, 50, doi: [10.1088/0004-637X/738/1/50](https://doi.org/10.1088/0004-637X/738/1/50)
- . 2012, ApJ, 757, 18, doi: [10.1088/0004-637X/757/1/18](https://doi.org/10.1088/0004-637X/757/1/18)
- Albrecht, S. H., Dawson, R. I., & Winn, J. N. 2022, PASP, 134, 082001, doi: [10.1088/1538-3873/ac6c09](https://doi.org/10.1088/1538-3873/ac6c09)
- Alonso, R., Brown, T. M., Torres, G., et al. 2004, ApJL, 613, L153, doi: [10.1086/425256](https://doi.org/10.1086/425256)
- Anderson, D. R., Brown, D. J. A., Collier Cameron, A., et al. 2014, arXiv e-prints, arXiv:1410.3449, doi: [10.48550/arXiv.1410.3449](https://doi.org/10.48550/arXiv.1410.3449)
- Anderson, D. R., Bouchy, F., Brown, D. J. A., et al. 2018, arXiv e-prints, arXiv:1812.09264, doi: [10.48550/arXiv.1812.09264](https://doi.org/10.48550/arXiv.1812.09264)
- Anderson, K. R., Winn, J. N., & Penev, K. 2021, ApJ, 914, 56, doi: [10.3847/1538-4357/abf8af](https://doi.org/10.3847/1538-4357/abf8af)
- Bakos, G., Noyes, R. W., Kovács, G., et al. 2004, PASP, 116, 266, doi: [10.1086/382735](https://doi.org/10.1086/382735)
- Bakos, G. Á., Csubry, Z., Penev, K., et al. 2013, PASP, 125, 154, doi: [10.1086/669529](https://doi.org/10.1086/669529)
- Bashi, D., Helled, R., Zucker, S., & Mordasini, C. 2017, A&A, 604, A83, doi: [10.1051/0004-6361/201629922](https://doi.org/10.1051/0004-6361/201629922)
- Bate, M. R. 2018, MNRAS, 475, 5618, doi: [10.1093/mnras/sty169](https://doi.org/10.1093/mnras/sty169)
- Bate, M. R., Lodato, G., & Pringle, J. E. 2010, MNRAS, 401, 1505, doi: [10.1111/j.1365-2966.2009.15773.x](https://doi.org/10.1111/j.1365-2966.2009.15773.x)
- Batygin, K. 2012, Nature, 491, 418, doi: [10.1038/nature11560](https://doi.org/10.1038/nature11560)
- Beaugé, C., & Nesvorný, D. 2012, ApJ, 751, 119, doi: [10.1088/0004-637X/751/2/119](https://doi.org/10.1088/0004-637X/751/2/119)
- Bieryla, A., Zhou, G., García-Mejía, J., et al. 2024, MNRAS, 527, 10955, doi: [10.1093/mnras/stad3785](https://doi.org/10.1093/mnras/stad3785)
- Blanco-Cuaresma, S. 2019, MNRAS, 486, 2075, doi: [10.1093/mnras/stz549](https://doi.org/10.1093/mnras/stz549)
- Blanco-Cuaresma, S., Soubiran, C., Heiter, U., & Jofré, P. 2014, A&A, 569, A111, doi: [10.1051/0004-6361/201423945](https://doi.org/10.1051/0004-6361/201423945)

<sup>15</sup> <https://adg.univie.ac.at/schwarz/intro.html>



- Borderies, N., Goldreich, P., & Tremaine, S. 1984, *ApJ*, 284, 429, doi: [10.1086/162423](https://doi.org/10.1086/162423)
- Borucki, W. J., Koch, D., Basri, G., et al. 2010, *Science*, 327, 977, doi: [10.1126/science.1185402](https://doi.org/10.1126/science.1185402)
- Bouchy, F., Queloz, D., Deleuil, M., et al. 2008, *A&A*, 482, L25, doi: [10.1051/0004-6361:200809433](https://doi.org/10.1051/0004-6361:200809433)
- Bourrier, V., Lecavelier des Etangs, A., Hébrard, G., et al. 2015, *A&A*, 579, A55, doi: [10.1051/0004-6361/201525750](https://doi.org/10.1051/0004-6361/201525750)
- Bowler, B. P., Tran, Q. H., Zhang, Z., et al. 2023, *AJ*, 165, 164, doi: [10.3847/1538-3881/acbd34](https://doi.org/10.3847/1538-3881/acbd34)
- Brahm, R., Espinoza, N., Jordán, A., et al. 2018, *MNRAS*, 477, 2572, doi: [10.1093/mnras/sty795](https://doi.org/10.1093/mnras/sty795)
- Brahm, R., Nielsen, L. D., Wittenmyer, R. A., et al. 2020, *AJ*, 160, 235, doi: [10.3847/1538-3881/abba3b](https://doi.org/10.3847/1538-3881/abba3b)
- Brown, D. J. A., Collier Cameron, A., Díaz, R. F., et al. 2012, *ApJ*, 760, 139, doi: [10.1088/0004-637X/760/2/139](https://doi.org/10.1088/0004-637X/760/2/139)
- Brown, T. M., Baliber, N., Bianco, F. B., et al. 2013, *PASP*, 125, 1031, doi: [10.1086/673168](https://doi.org/10.1086/673168)
- Butler, R. P., Marcy, G. W., Williams, E., et al. 1996, *Publications of the Astronomical Society of the Pacific*, 108, 500
- Caldwell, D. A., Tenenbaum, P., Twicken, J. D., et al. 2020, *Research Notes of the American Astronomical Society*, 4, 201, doi: [10.3847/2515-5172/abc9b3](https://doi.org/10.3847/2515-5172/abc9b3)
- Carleo, I., Barrágan, O., Persson, C. M., et al. 2024, arXiv e-prints, arXiv:2408.05612, doi: [10.48550/arXiv.2408.05612](https://doi.org/10.48550/arXiv.2408.05612)
- Chen, J., & Kipping, D. 2017, *ApJ*, 834, 17, doi: [10.3847/1538-4357/834/1/17](https://doi.org/10.3847/1538-4357/834/1/17)
- Choi, J., Dotter, A., Conroy, C., et al. 2016, *ApJ*, 823, 102, doi: [10.3847/0004-637X/823/2/102](https://doi.org/10.3847/0004-637X/823/2/102)
- Collins, K. 2019, in *American Astronomical Society Meeting Abstracts*, Vol. 233, American Astronomical Society Meeting Abstracts #233, 140.05
- Collins, K. A., Kielkopf, J. F., Stassun, K. G., & Hessman, F. V. 2017, *AJ*, 153, 77, doi: [10.3847/1538-3881/153/2/77](https://doi.org/10.3847/1538-3881/153/2/77)
- Crane, J. D., Shectman, S. A., & Butler, R. P. 2006, in *Society of Photo-Optical Instrumentation Engineers (SPIE) Conference Series*, Vol. 6269, Society of Photo-Optical Instrumentation Engineers (SPIE) Conference Series, ed. I. S. McLean & M. Iye, 626931, doi: [10.1117/12.672339](https://doi.org/10.1117/12.672339)
- Crane, J. D., Shectman, S. A., Butler, R. P., et al. 2010, in *Ground-based and Airborne Instrumentation for Astronomy III*, Vol. 7735, SPIE, 1909–1923
- Crane, J. D., Shectman, S. A., Butler, R. P., Thompson, I. B., & Burley, G. S. 2008, in *Ground-based and Airborne Instrumentation for Astronomy II*, Vol. 7014, SPIE, 2484–2493
- Cutri, R. M., Skrutskie, M. F., van Dyk, S., et al. 2003, *VizieR Online Data Catalog*, II/246
- Cutri, R. M., Wright, E. L., Conrow, T., et al. 2021, *VizieR Online Data Catalog*, II/328
- Damiani, C., & Mathis, S. 2018, *A&A*, 618, A90, doi: [10.1051/0004-6361/201732538](https://doi.org/10.1051/0004-6361/201732538)
- Davies, C. L. 2019, *MNRAS*, 484, 1926
- Dawson, R. I., & Johnson, J. A. 2018, *ARA&A*, 56, 175, doi: [10.1146/annurev-astro-081817-051853](https://doi.org/10.1146/annurev-astro-081817-051853)
- de Laplace, P. S. 1796, *Exposition du système du monde*, doi: [10.3931/e-rara-497](https://doi.org/10.3931/e-rara-497)
- Djupvik, A. A., & Andersen, J. 2010, in *Astrophysics and Space Science Proceedings*, Vol. 14, Highlights of Spanish Astrophysics V, 211, doi: [10.1007/978-3-642-11250-8\\_21](https://doi.org/10.1007/978-3-642-11250-8_21)
- Dong, J., & Foreman-Mackey, D. 2023, arXiv e-prints, arXiv:2305.14220, doi: [10.48550/arXiv.2305.14220](https://doi.org/10.48550/arXiv.2305.14220)
- Dong, J., Huang, C. X., Dawson, R. I., et al. 2021, *ApJS*, 255, 6, doi: [10.3847/1538-4365/abf73c](https://doi.org/10.3847/1538-4365/abf73c)
- Dong, J., Wang, S., Rice, M., et al. 2023, *ApJL*, 951, L29, doi: [10.3847/2041-8213/acd93d](https://doi.org/10.3847/2041-8213/acd93d)
- Dotter, A. 2016, *ApJS*, 222, 8, doi: [10.3847/0067-0049/222/1/8](https://doi.org/10.3847/0067-0049/222/1/8)
- Doyle, A. P., Davies, G. R., Smalley, B., Chaplin, W. J., & Elsworth, Y. 2014, *MNRAS*, 444, 3592, doi: [10.1093/mnras/stu1692](https://doi.org/10.1093/mnras/stu1692)
- Eastman, J. 2017, EXOFASTv2: Generalized publication-quality exoplanet modeling code. <http://ascl.net/1710.003>
- Eastman, J. D., Rodriguez, J. E., Agol, E., et al. 2019, arXiv e-prints, arXiv:1907.09480. <https://arxiv.org/abs/1907.09480>
- Eberhardt, J., Hobson, M. J., Henning, T., et al. 2023, *AJ*, 166, 271, doi: [10.3847/1538-3881/ad06bc](https://doi.org/10.3847/1538-3881/ad06bc)
- El-Badry, K., Rix, H.-W., & Heintz, T. M. 2021, *MNRAS*, 506, 2269, doi: [10.1093/mnras/stab323](https://doi.org/10.1093/mnras/stab323)
- Espinoza-Retamal, J. I., Brahm, R., Petrovich, C., et al. 2024, in prep
- . 2023, *ApJL*, 958, L20, doi: [10.3847/2041-8213/ad096d](https://doi.org/10.3847/2041-8213/ad096d)
- Fabrycky, D., & Tremaine, S. 2007, *ApJ*, 669, 1298, doi: [10.1086/521702](https://doi.org/10.1086/521702)
- Ferreira, T., Rice, M., Wang, X.-Y., & Wang, S. 2024, arXiv e-prints, arXiv:2408.00725, doi: [10.48550/arXiv.2408.00725](https://doi.org/10.48550/arXiv.2408.00725)
- Fielding, D. B., McKee, C. F., Socrates, A., Cunningham, A. J., & Klein, R. I. 2015, *MNRAS*, 450, 3306, doi: [10.1093/mnras/stv836](https://doi.org/10.1093/mnras/stv836)
- Fontanive, C., & Bardalez Gagliuffi, D. 2021, *Frontiers in Astronomy and Space Sciences*, 8, 16, doi: [10.3389/fspas.2021.625250](https://doi.org/10.3389/fspas.2021.625250)

- Foreman-Mackey, D., Hogg, D. W., Lang, D., & Goodman, J. 2013, *PASP*, 125, 306, doi: [10.1086/670067](https://doi.org/10.1086/670067)
- Foucart, F., & Lai, D. 2011, *MNRAS*, 412, 2799, doi: [10.1111/j.1365-2966.2010.18176.x](https://doi.org/10.1111/j.1365-2966.2010.18176.x)
- Franson, K., Bowler, B. P., Zhou, Y., et al. 2023, *ApJL*, 950, L19, doi: [10.3847/2041-8213/acd6f6](https://doi.org/10.3847/2041-8213/acd6f6)
- Fulton, B. J., Petigura, E. A., Blunt, S., & Sinukoff, E. 2018, *PASP*, 130, 044504, doi: [10.1088/1538-3873/aaaaa8](https://doi.org/10.1088/1538-3873/aaaaa8)
- Fulton, B. J., Howard, A. W., Winn, J. N., et al. 2013, *ApJ*, 772, 80, doi: [10.1088/0004-637X/772/2/80](https://doi.org/10.1088/0004-637X/772/2/80)
- Furész, G., Szentgyorgyi, A., Latham, D., & Vinkó, J. 2008, PhD thesis, Ph. D. thesis, University of Szeged, Hungary
- Gaia Collaboration, Vallenari, A., Brown, A. G. A., et al. 2023, *A&A*, 674, A1, doi: [10.1051/0004-6361/202243940](https://doi.org/10.1051/0004-6361/202243940)
- Gan, T., Wang, S. X., Dai, F., et al. 2024, *ApJL*, 969, L24, doi: [10.3847/2041-8213/ad5967](https://doi.org/10.3847/2041-8213/ad5967)
- Gelman, A., & Rubin, D. B. 1992, *Statistical Science*, 7, 457, doi: [10.1214/ss/1177011136](https://doi.org/10.1214/ss/1177011136)
- Giles, H. A. C., Bayliss, D., Espinoza, N., et al. 2018, *MNRAS*, 475, 1809, doi: [10.1093/mnras/stx3300](https://doi.org/10.1093/mnras/stx3300)
- Gray, R. O., & Corbally, C. J. 1994, *AJ*, 107, 742, doi: [10.1086/116893](https://doi.org/10.1086/116893)
- Guenther, E. W., Díaz, R. F., Gazzano, J. C., et al. 2012, *A&A*, 537, A136, doi: [10.1051/0004-6361/201117706](https://doi.org/10.1051/0004-6361/201117706)
- Guerrero, N. M., Seager, S., Huang, C. X., et al. 2021, *ApJS*, 254, 39, doi: [10.3847/1538-4365/abefe1](https://doi.org/10.3847/1538-4365/abefe1)
- Günther, M. N., & Daylan, T. 2019, *Allesfitter: Flexible Star and Exoplanet Inference From Photometry and Radial Velocity*, *Astrophysics Source Code Library*. <http://ascl.net/1903.003>
- . 2021, *ApJS*, 254, 13, doi: [10.3847/1538-4365/abe70e](https://doi.org/10.3847/1538-4365/abe70e)
- Gustafsson, B., Edvardsson, B., Eriksson, K., et al. 2008, *A&A*, 486, 951, doi: [10.1051/0004-6361:200809724](https://doi.org/10.1051/0004-6361:200809724)
- Halverson, S., Terrien, R., Mahadevan, S., et al. 2016, in *Society of Photo-Optical Instrumentation Engineers (SPIE) Conference Series*, Vol. 9908, *Ground-based and Airborne Instrumentation for Astronomy VI*, ed. C. J. Evans, L. Simard, & H. Takami, 99086P, doi: [10.1117/12.2232761](https://doi.org/10.1117/12.2232761)
- Harre, J.-V., Smith, A. M. S., Hirano, T., et al. 2023, *AJ*, 166, 159, doi: [10.3847/1538-3881/acf46d](https://doi.org/10.3847/1538-3881/acf46d)
- Harris, C. R., Millman, K. J., van der Walt, S. J., et al. 2020, *Nature*, 585, 357
- Hatzes, A. P., & Rauer, H. 2015, *ApJL*, 810, L25, doi: [10.1088/2041-8205/810/2/L25](https://doi.org/10.1088/2041-8205/810/2/L25)
- Heiter, U., Lind, K., Bergemann, M., et al. 2021, *A&A*, 645, A106, doi: [10.1051/0004-6361/201936291](https://doi.org/10.1051/0004-6361/201936291)
- Helled, R. 2023, *A&A*, 675, L8, doi: [10.1051/0004-6361/202346850](https://doi.org/10.1051/0004-6361/202346850)
- Hippke, M., David, T. J., Mulders, G. D., & Heller, R. 2019, *AJ*, 158, 143, doi: [10.3847/1538-3881/ab3984](https://doi.org/10.3847/1538-3881/ab3984)
- Hirano, T., Suto, Y., Winn, J. N., et al. 2011, *ApJ*, 742, 69, doi: [10.1088/0004-637X/742/2/69](https://doi.org/10.1088/0004-637X/742/2/69)
- Hixenbaugh, K., Wang, X.-Y., Rice, M., & Wang, S. 2023, *ApJL*, 949, L35, doi: [10.3847/2041-8213/acd6f5](https://doi.org/10.3847/2041-8213/acd6f5)
- Hjorth, M., Albrecht, S., Hirano, T., et al. 2021, *Proceedings of the National Academy of Science*, 118, e2017418118, doi: [10.1073/pnas.2017418118](https://doi.org/10.1073/pnas.2017418118)
- Hodges, J. L. 1958, *Arkiv för Matematik*, 3, 469. <https://api.semanticscholar.org/CorpusID:121451525>
- Holcomb, R. J., Robertson, P., Hartigan, P., Oelkers, R. J., & Robinson, C. 2022, *ApJ*, 936, 138, doi: [10.3847/1538-4357/ac8990](https://doi.org/10.3847/1538-4357/ac8990)
- Howell, S. B., Sobek, C., Haas, M., et al. 2014, *PASP*, 126, 398, doi: [10.1086/676406](https://doi.org/10.1086/676406)
- Hu, Q., Rice, M., Wang, X.-Y., et al. 2024, *AJ*, 167, 175, doi: [10.3847/1538-3881/ad2855](https://doi.org/10.3847/1538-3881/ad2855)
- Huang, C. X., Vanderburg, A., Pál, A., et al. 2020a, *Research Notes of the American Astronomical Society*, 4, 204, doi: [10.3847/2515-5172/abca2e](https://doi.org/10.3847/2515-5172/abca2e)
- . 2020b, *Research Notes of the American Astronomical Society*, 4, 206, doi: [10.3847/2515-5172/abca2d](https://doi.org/10.3847/2515-5172/abca2d)
- Hunter, J. D. 2007, *Computing in science & engineering*, 9, 90
- Hurt, S. A., & MacGregor, M. A. 2023, *ApJ*, 954, 10
- Hut, P. 1981, *A&A*, 99, 126
- Ikwut-Ukwa, M., Rodriguez, J. E., Quinn, S. N., et al. 2022, *AJ*, 163, 9, doi: [10.3847/1538-3881/ac2ee1](https://doi.org/10.3847/1538-3881/ac2ee1)
- Jenkins, J. M., Twicken, J. D., McCauliff, S., et al. 2016, in *Society of Photo-Optical Instrumentation Engineers (SPIE) Conference Series*, Vol. 9913, *Software and Cyberinfrastructure for Astronomy IV*, ed. G. Chiozzi & J. C. Guzman, 99133E, doi: [10.1117/12.2233418](https://doi.org/10.1117/12.2233418)
- Jensen, E. 2013a, *Tapir: A web interface for transit/eclipse observability*, *Astrophysics Source Code Library*, record ascl:1306.007
- . 2013b, *Tapir: A web interface for transit/eclipse observability*, *Astrophysics Source Code Library*. <http://ascl.net/1306.007>
- Jofré, P., Heiter, U., Soubiran, C., et al. 2014, *A&A*, 564, A133, doi: [10.1051/0004-6361/201322440](https://doi.org/10.1051/0004-6361/201322440)
- Johnson, M. C., Cochran, W. D., Addison, B. C., Tinney, C. G., & Wright, D. J. 2017, *AJ*, 154, 137, doi: [10.3847/1538-3881/aa8462](https://doi.org/10.3847/1538-3881/aa8462)

- Kanodia, S., Mahadevan, S., Ramsey, L. W., et al. 2018, in Society of Photo-Optical Instrumentation Engineers (SPIE) Conference Series, Vol. 10702, Ground-based and Airborne Instrumentation for Astronomy VII, ed. C. J. Evans, L. Simard, & H. Takami, 107026Q, doi: [10.1117/12.2313491](https://doi.org/10.1117/12.2313491)
- Kanodia, S., Lin, A. S. J., Lubar, E., et al. 2023, AJ, 166, 105, doi: [10.3847/1538-3881/acea60](https://doi.org/10.3847/1538-3881/acea60)
- Kant, I. 1755, Allgemeine Naturgeschichte und Theorie des Himmels
- Kipping, D. M. 2013, MNRAS, 435, 2152, doi: [10.1093/mnras/stt1435](https://doi.org/10.1093/mnras/stt1435)
- Knudstrup, E., & Albrecht, S. H. 2022, A&A, 660, A99, doi: [10.1051/0004-6361/202142726](https://doi.org/10.1051/0004-6361/202142726)
- Knudstrup, E., Albrecht, S. H., Winn, J. N., et al. 2024, in revision, A&A
- Knudstrup, E., Serrano, L. M., Gandolfi, D., et al. 2022, A&A, 667, A22, doi: [10.1051/0004-6361/202243656](https://doi.org/10.1051/0004-6361/202243656)
- Kraft, R. P. 1967, ApJ, 150, 551, doi: [10.1086/149359](https://doi.org/10.1086/149359)
- Kraus, S., Le Bouquin, J.-B., Kreplin, A., et al. 2020, ApJL, 897, L8, doi: [10.3847/2041-8213/ab9d27](https://doi.org/10.3847/2041-8213/ab9d27)
- Lai, D. 2012, MNRAS, 423, 486, doi: [10.1111/j.1365-2966.2012.20893.x](https://doi.org/10.1111/j.1365-2966.2012.20893.x)
- Lai, D., Foucart, F., & Lin, D. N. C. 2011, MNRAS, 412, 2790, doi: [10.1111/j.1365-2966.2010.18127.x](https://doi.org/10.1111/j.1365-2966.2010.18127.x)
- Li, G., & Winn, J. N. 2016, ApJ, 818, 5, doi: [10.3847/0004-637X/818/1/5](https://doi.org/10.3847/0004-637X/818/1/5)
- Lin, Y., & Ogilvie, G. I. 2017, MNRAS, 468, 1387, doi: [10.1093/mnras/stx540](https://doi.org/10.1093/mnras/stx540)
- Lubin, J., Wang, X.-Y., Rice, M., et al. 2023, ApJL, 959, L5, doi: [10.3847/2041-8213/ad0fea](https://doi.org/10.3847/2041-8213/ad0fea)
- Lubow, S. H., & Ogilvie, G. I. 2000, ApJ, 538, 326, doi: [10.1086/309101](https://doi.org/10.1086/309101)
- Mancini, L., Esposito, M., Covino, E., et al. 2022, A&A, 664, A162, doi: [10.1051/0004-6361/202243742](https://doi.org/10.1051/0004-6361/202243742)
- Markwardt, C. B. 2009, in Astronomical Society of the Pacific Conference Series, Vol. 411, Astronomical Data Analysis Software and Systems XVIII, ed. D. A. Bohlander, D. Durand, & P. Dowler, 251. <https://arxiv.org/abs/0902.2850>
- Matsakos, T., & Königl, A. 2017, AJ, 153, 60, doi: [10.3847/1538-3881/153/2/60](https://doi.org/10.3847/1538-3881/153/2/60)
- McCullough, P. R., Stys, J. E., Valenti, J. A., et al. 2005, Publications of the Astronomical Society of the Pacific, 117, 783, doi: [10.1086/432024](https://doi.org/10.1086/432024)
- McCully, C., Volgenau, N. H., Harbeck, D.-R., et al. 2018, in Society of Photo-Optical Instrumentation Engineers (SPIE) Conference Series, Vol. 10707, Software and Cyberinfrastructure for Astronomy V, ed. J. C. Guzman & J. Ibsen, 107070K, doi: [10.1117/12.2314340](https://doi.org/10.1117/12.2314340)
- McKinney, W. 2010, in Proceedings of the 9th Python in Science Conference, Vol. 445, Austin, TX, 51–56
- Morgan, M., Bowler, B. P., Tran, Q. H., et al. 2024, AJ, 167, 48, doi: [10.3847/1538-3881/ad0728](https://doi.org/10.3847/1538-3881/ad0728)
- Müller, S., Baron, J., Helled, R., Bouchy, F., & Parc, L. 2024, A&A, 686, A296, doi: [10.1051/0004-6361/202348690](https://doi.org/10.1051/0004-6361/202348690)
- Naoz, S. 2016, ARA&A, 54, 441, doi: [10.1146/annurev-astro-081915-023315](https://doi.org/10.1146/annurev-astro-081915-023315)
- Naoz, S., Farr, W. M., & Rasio, F. A. 2012, The Astrophysical Journal Letters, 754, L36
- Ogilvie, G. I., & Lin, D. N. C. 2007, ApJ, 661, 1180, doi: [10.1086/515435](https://doi.org/10.1086/515435)
- Oliphant, T. E. 2006, A guide to NumPy, Vol. 1 (Trelgol Publishing USA)
- Parviainen, H. 2015, MNRAS, 450, 3233, doi: [10.1093/mnras/stv894](https://doi.org/10.1093/mnras/stv894)
- Parviainen, H. 2015, MNRAS, 450, 3233, doi: [10.1093/mnras/stv894](https://doi.org/10.1093/mnras/stv894)
- Pepper, J., Pogge, R., Depoy, D. L., et al. 2007, Astronomical Society of the Pacific Conference Series, Vol. 366, Early Results from the KELT Transit Survey, ed. C. Afonso, D. Wel Drake, & T. Henning, 27
- Petrovich, C. 2015a, ApJ, 799, 27, doi: [10.1088/0004-637X/799/1/27](https://doi.org/10.1088/0004-637X/799/1/27)
- . 2015b, ApJ, 805, 75, doi: [10.1088/0004-637X/805/1/75](https://doi.org/10.1088/0004-637X/805/1/75)
- Pollacco, D. L., Skillen, I., Collier Cameron, A., et al. 2006, PASP, 118, 1407, doi: [10.1086/508556](https://doi.org/10.1086/508556)
- Pont, F., Endl, M., Cochran, W. D., et al. 2010, MNRAS, 402, L1, doi: [10.1111/j.1745-3933.2009.00785.x](https://doi.org/10.1111/j.1745-3933.2009.00785.x)
- Prinath, B., Sedaghati, E., Seidel, J. V., et al. 2024, arXiv e-prints, arXiv:2406.08558, doi: [10.48550/arXiv.2406.08558](https://doi.org/10.48550/arXiv.2406.08558)
- Radzom, B. T., Dong, J., Rice, M., et al. 2024, arXiv e-prints, arXiv:2404.06504, doi: [10.48550/arXiv.2404.06504](https://doi.org/10.48550/arXiv.2404.06504)
- Rasio, F. A., & Ford, E. B. 1996, Science, 274, 954, doi: [10.1126/science.274.5289.954](https://doi.org/10.1126/science.274.5289.954)
- Rice, M., Wang, S., Gerbig, K., et al. 2023a, AJ, 165, 65, doi: [10.3847/1538-3881/aca88e](https://doi.org/10.3847/1538-3881/aca88e)
- Rice, M., Wang, S., & Laughlin, G. 2022a, ApJL, 926, L17, doi: [10.3847/2041-8213/ac502d](https://doi.org/10.3847/2041-8213/ac502d)
- Rice, M., Wang, S., Howard, A. W., et al. 2021, AJ, 162, 182, doi: [10.3847/1538-3881/ac1f8f](https://doi.org/10.3847/1538-3881/ac1f8f)
- Rice, M., Wang, S., Wang, X.-Y., et al. 2022b, AJ, 164, 104, doi: [10.3847/1538-3881/ac8153](https://doi.org/10.3847/1538-3881/ac8153)
- Rice, M., Wang, X.-Y., Wang, S., et al. 2023b, AJ, 166, 266, doi: [10.3847/1538-3881/ad09de](https://doi.org/10.3847/1538-3881/ad09de)

- Ricker, G. R., Winn, J. N., Vanderspek, R., et al. 2015, *Journal of Astronomical Telescopes, Instruments, and Systems*, 1, 014003, doi: [10.1117/1.JATIS.1.1.014003](https://doi.org/10.1117/1.JATIS.1.1.014003)
- Robertson, P., Anderson, T., Stefansson, G., et al. 2019, *Journal of Astronomical Telescopes, Instruments, and Systems*, 5, 015003, doi: [10.1117/1.JATIS.5.1.015003](https://doi.org/10.1117/1.JATIS.5.1.015003)
- Rodriguez, J. E., Quinn, S. N., Zhou, G., et al. 2021, *AJ*, 161, 194, doi: [10.3847/1538-3881/abe38a](https://doi.org/10.3847/1538-3881/abe38a)
- Rodriguez, J. E., Quinn, S. N., Vanderburg, A., et al. 2023, *MNRAS*, 521, 2765, doi: [10.1093/mnras/stad595](https://doi.org/10.1093/mnras/stad595)
- Rogers, T. M., & Lin, D. N. C. 2013, *ApJL*, 769, L10, doi: [10.1088/2041-8205/769/1/L10](https://doi.org/10.1088/2041-8205/769/1/L10)
- Romanova, M. M., Koldoba, A. V., Ustyugova, G. V., et al. 2021, *MNRAS*, 506, 372, doi: [10.1093/mnras/stab1724](https://doi.org/10.1093/mnras/stab1724)
- Romanova, M. M., Ustyugova, G. V., Koldoba, A. V., & Lovelace, R. V. E. 2013, *MNRAS*, 430, 699, doi: [10.1093/mnras/sts670](https://doi.org/10.1093/mnras/sts670)
- Schlafly, E. F., & Finkbeiner, D. P. 2011, *ApJ*, 737, 103, doi: [10.1088/0004-637X/737/2/103](https://doi.org/10.1088/0004-637X/737/2/103)
- Schlaufman, K. C. 2010, *ApJ*, 719, 602, doi: [10.1088/0004-637X/719/1/602](https://doi.org/10.1088/0004-637X/719/1/602)
- Scholz, F. W., & Stephens, M. A. 1987, *Journal of the American Statistical Association*, 82, 918
- Schulte, J., Rodriguez, J. E., & Others. 2024, in prep
- Schwab, C., Rakich, A., Gong, Q., et al. 2016, in *Society of Photo-Optical Instrumentation Engineers (SPIE) Conference Series*, Vol. 9908, *Ground-based and Airborne Instrumentation for Astronomy VI*, ed. C. J. Evans, L. Simard, & H. Takami, 99087H, doi: [10.1117/12.2234411](https://doi.org/10.1117/12.2234411)
- Schwarz, R., Funk, B., Zechner, R., & Bazsó, Á. 2016, *Monthly Notices of the Royal Astronomical Society*, 460, 3598
- Sedaghati, E., Jordán, A., Brahm, R., et al. 2023, *AJ*, 166, 130, doi: [10.3847/1538-3881/acea84](https://doi.org/10.3847/1538-3881/acea84)
- Sepulveda, A. G., Huber, D., Bedding, T. R., et al. 2024, *AJ*, 168, 13, doi: [10.3847/1538-3881/ad4964](https://doi.org/10.3847/1538-3881/ad4964)
- Shporer, A., Zhou, G., Fulton, B. J., et al. 2017, *AJ*, 154, 188, doi: [10.3847/1538-3881/aa8bb9](https://doi.org/10.3847/1538-3881/aa8bb9)
- Siegel, J. C., Winn, J. N., & Albrecht, S. H. 2023, *ApJL*, 950, L2, doi: [10.3847/2041-8213/acd62f](https://doi.org/10.3847/2041-8213/acd62f)
- Simpson, E. K., Pollacco, D., Cameron, A. C., et al. 2011, *MNRAS*, 414, 3023, doi: [10.1111/j.1365-2966.2011.18603.x](https://doi.org/10.1111/j.1365-2966.2011.18603.x)
- Smith, A. M. S., Anderson, D. R., Collier Cameron, A., et al. 2012, *AJ*, 143, 81, doi: [10.1088/0004-6256/143/4/81](https://doi.org/10.1088/0004-6256/143/4/81)
- Smith, A. M. S., Gandolfi, D., Barragán, O., et al. 2017, *MNRAS*, 464, 2708, doi: [10.1093/mnras/stw2487](https://doi.org/10.1093/mnras/stw2487)
- Southworth, J. 2011, *MNRAS*, 417, 2166, doi: [10.1111/j.1365-2966.2011.19399.x](https://doi.org/10.1111/j.1365-2966.2011.19399.x)
- Spalding, C., & Winn, J. N. 2022, *ApJ*, 927, 22, doi: [10.3847/1538-4357/ac4993](https://doi.org/10.3847/1538-4357/ac4993)
- Stefansson, G., Hearty, F., Robertson, P., et al. 2016, *ApJ*, 833, 175, doi: [10.3847/1538-4357/833/2/175](https://doi.org/10.3847/1538-4357/833/2/175)
- Storn, R., & Price, K. V. 1997, *Journal of Global Optimization*, 11, 341, <https://api.semanticscholar.org/CorpusID:5297867>
- Stumpe, M. C., Smith, J. C., Catanzarite, J. H., et al. 2014, *PASP*, 126, 100, doi: [10.1086/674989](https://doi.org/10.1086/674989)
- Stumpe, M. C., Smith, J. C., Van Cleve, J. E., et al. 2012, *PASP*, 124, 985, doi: [10.1086/667698](https://doi.org/10.1086/667698)
- Tayar, J., Claytor, Z. R., Huber, D., & van Saders, J. 2022, *ApJ*, 927, 31, doi: [10.3847/1538-4357/ac4bbc](https://doi.org/10.3847/1538-4357/ac4bbc)
- Telting, J., Avila, G., Buchhave, L., et al. 2014, *Astronomische Nachrichten*, 335, 41
- Telting, J. H., Avila, G., Buchhave, L., et al. 2014, *Astronomische Nachrichten*, 335, 41, doi: [10.1002/asna.201312007](https://doi.org/10.1002/asna.201312007)
- Thies, I., Kroupa, P., Goodwin, S. P., Stamatellos, D., & Whitworth, A. P. 2011, *MNRAS*, 417, 1817, doi: [10.1111/j.1365-2966.2011.19390.x](https://doi.org/10.1111/j.1365-2966.2011.19390.x)
- Tokovinin, A., Fischer, D. A., Bonati, M., et al. 2013, *PASP*, 125, 1336, doi: [10.1086/674012](https://doi.org/10.1086/674012)
- TriAUD, A. H. M. J. 2018, in *Handbook of Exoplanets*, ed. H. J. Deeg & J. A. Belmonte, 2, doi: [10.1007/978-3-319-55333-7\\_2](https://doi.org/10.1007/978-3-319-55333-7_2)
- TriAUD, A. H. M. J., Collier Cameron, A., Queloz, D., et al. 2010, *A&A*, 524, A25, doi: [10.1051/0004-6361/201014525](https://doi.org/10.1051/0004-6361/201014525)
- TriAUD, A. H. M. J., Queloz, D., Hellier, C., et al. 2011, *A&A*, 531, A24, doi: [10.1051/0004-6361/201016367](https://doi.org/10.1051/0004-6361/201016367)
- Valsecchi, F., & Rasio, F. A. 2014, *ApJ*, 786, 102, doi: [10.1088/0004-637X/786/2/102](https://doi.org/10.1088/0004-637X/786/2/102)
- Virtanen, P., Gommers, R., Oliphant, T. E., et al. 2020, *Nature methods*, 17, 261
- Walt, S. v. d., Colbert, S. C., & Varoquaux, G. 2011, *Computing in Science & Engineering*, 13, 22
- Wang, S., Zhang, H., Zhou, J.-L., et al. 2014, *ApJS*, 211, 26, doi: [10.1088/0067-0049/211/2/26](https://doi.org/10.1088/0067-0049/211/2/26)
- Wang, S., Winn, J. N., Addison, B. C., et al. 2021, *AJ*, 162, 50, doi: [10.3847/1538-3881/ac0626](https://doi.org/10.3847/1538-3881/ac0626)
- Wang, X.-Y., Rice, M., Wang, S., et al. 2022, *ApJL*, 926, L8, doi: [10.3847/2041-8213/ac4f44](https://doi.org/10.3847/2041-8213/ac4f44)
- Weiss, L. M., & Marcy, G. W. 2014, *ApJL*, 783, L6, doi: [10.1088/2041-8205/783/1/L6](https://doi.org/10.1088/2041-8205/783/1/L6)
- Winn, J. N., Fabrycky, D., Albrecht, S., & Johnson, J. A. 2010, *ApJL*, 718, L145, doi: [10.1088/2041-8205/718/2/L145](https://doi.org/10.1088/2041-8205/718/2/L145)
- Winn, J. N., & Fabrycky, D. C. 2015, *ARA&A*, 53, 409, doi: [10.1146/annurev-astro-082214-122246](https://doi.org/10.1146/annurev-astro-082214-122246)

- Wright, J., Rice, M., Wang, X.-Y., Hixenbaugh, K., & Wang, S. 2023, *AJ*, 166, 217, doi: [10.3847/1538-3881/ad0131](https://doi.org/10.3847/1538-3881/ad0131)
- Wu, D.-H., Rice, M., & Wang, S. 2023, *AJ*, 165, 171, doi: [10.3847/1538-3881/acbf3f](https://doi.org/10.3847/1538-3881/acbf3f)
- Wu, Y., & Lithwick, Y. 2011, *ApJ*, 735, 109, doi: [10.1088/0004-637X/735/2/109](https://doi.org/10.1088/0004-637X/735/2/109)
- Wu, Y., & Murray, N. 2003, *ApJ*, 589, 605, doi: [10.1086/374598](https://doi.org/10.1086/374598)
- Wytttenbach, A., Lovis, C., Ehrenreich, D., et al. 2017, *A&A*, 602, A36, doi: [10.1051/0004-6361/201630063](https://doi.org/10.1051/0004-6361/201630063)
- Xue, Y., Suto, Y., Taruya, A., et al. 2014, *ApJ*, 784, 66, doi: [10.1088/0004-637X/784/1/66](https://doi.org/10.1088/0004-637X/784/1/66)
- Yee, S. W., Winn, J., Hartman, J., et al. 2024, in prep
- Zanazzi, J. J., Dewberry, J., & Chiang, E. 2024, *ApJL*, 967, L29, doi: [10.3847/2041-8213/ad4644](https://doi.org/10.3847/2041-8213/ad4644)
- Zechmeister, M., & Kürster, M. 2009, *A&A*, 496, 577, doi: [10.1051/0004-6361:200811296](https://doi.org/10.1051/0004-6361:200811296)
- Zhou, G., Bayliss, D., Hartman, J. D., et al. 2015, *ApJL*, 814, L16, doi: [10.1088/2041-8205/814/1/L16](https://doi.org/10.1088/2041-8205/814/1/L16)